

December 11, 2001

MEMORANDUM TO: Dr. John T. Larkins, Executive Director
Advisory Committee on Reactor Safeguards

FROM: Jack R. Strosnider, Director */ra by FEltawila f/*
Division of Engineering
Office of Nuclear Reactor Regulation

SUBJECT: NON-PROPRIETARY VERSION OF THE STAFF PRELIMINARY
TECHNICAL ASSESSMENT OF REACTOR PRESSURE VESSEL
HEAD PENETRATION NOZZLE CRACKING

By memorandum dated November 6, 2001, I sent to you a preliminary technical assessment (PTA) on reactor pressure vessel head penetration nozzle cracking, as related to NRC Bulletin 2001-01, "Circumferential Cracking of Reactor Pressure Vessel Head Penetration Nozzles." Attached to the memorandum was a non-proprietary version of the PTA that included little of the technical details due to our concerns regarding the potential for disclosure of proprietary information in the assessment. We have recently received permission from the appropriate groups to release the sections of the report dealing with the proprietary material, subject to minor modifications to the references in Section 9 of the report. We have made the necessary modifications to Section 9 of the report, and a complete, non-proprietary version of the report is attached.

The PTA was discussed in detail with the Advisory Committee on Reactor Safeguards (ACRS) on November 9, 2001. This assessment represents our best characterization of this issue at this time. The staff continues to engage the industry and gather additional information regarding VHP nozzle inspection results and the various technical aspects related to this cracking issue, and we will continue to update our assessment.

If you have any questions regarding this report or related issues, please contact Allen Hiser of my staff.

Attachment: As stated

cc w/attachment: See next page

CONTACT: Allen Hiser, EMC/DE
(301) 415-1034

MEMORANDUM TO: Dr. John T. Larkins, Executive Director
Advisory Committee on Reactor Safeguards

FROM: Jack R. Strosnider, Director
Division of Engineering
Office of Nuclear Reactor Regulation

SUBJECT: NON-PROPRIETARY VERSION OF THE STAFF PRELIMINARY
TECHNICAL ASSESSMENT OF REACTOR PRESSURE VESSEL
HEAD PENETRATION NOZZLE CRACKING

By memorandum dated November 6, 2001, I sent to you a preliminary technical assessment (PTA) on reactor pressure vessel head penetration nozzle cracking, as related to NRC Bulletin 2001-01, "Circumferential Cracking of Reactor Pressure Vessel Head Penetration Nozzles." Attached to the memorandum was a non-proprietary version of the PTA that included little of the technical details due to our concerns regarding the potential for disclosure of proprietary information in the assessment. We have recently received permission from the appropriate groups to release the sections of the report dealing with the proprietary material, subject to minor modifications to the references in Section 9 of the report. We have made the necessary modifications to Section 9 of the report, and a complete, non-proprietary version of the report is attached.

The PTA was discussed in detail with the Advisory Committee on Reactor Safeguards (ACRS) on November 9, 2001. This assessment represents our best characterization of this issue at this time. The staff continues to engage the industry and gather additional information regarding VHP nozzle inspection results and the various technical aspects related to this cracking issue, and we will continue to update our assessment.

If you have any questions regarding this report or related issues, please contact Allen Hiser of my staff.

Attachments: As stated

cc w/attachment: See next page
CONTACT: Allen Hiser, EMCB/DE
(301) 415-1034

DISTRIBUTION:

| | | | |
|-------------------|------------|-----------|-----------------------|
| SCollins/JJohnson | JShea | RBarrett | EHackett |
| BSheron | SRosenberg | FReinhart | DLew, Region I |
| JZwolinski/TMarsh | MWeston | JChung | MLesser, Region II |
| GHolahan/SBlack | JZimmerman | MMayfield | MHolmberg, Region III |
| FElawila | ALee | NChokshi | CPaulk, Region IV |

DOCUMENT NAME: G:\HISER\PTA 12-04-01.wpd

INDICATE IN BOX: "C"=COPY W/O ATTACHMENT/ENCLOSURE, "E"=COPY W/ATT/ENCL, "N"=NO COPY

| | | | | |
|--------|-------------|---------------|---------------|--------------------|
| OFFICE | EMCB:DE | EMCB:DE | BC:EMCB | D:DE |
| NAME | ALHiser:alh | KRWichman:krw | WHBateman:whb | JRStrosnider:fe f/ |
| DATE | 12/ 04 /01 | 12/ 4 /01 | 12/ 5 /01 | 12/ 11 /01 |

OFFICIAL RECORD COPY

PACKAGE ACCESSION NO.: ML01

cc:

Ralph Beedle, Senior Vice President
and Chief Nuclear Officer
Alex Marion, Director of Engineering
Kurt Cozens
Nuclear Energy Institute
Suite 400
1776 I Street, NW
Washington, DC 20006-3708

Avtar Singh, EPRI MRP Manager
Chuck Welty, EPRI MRP Manager
Allan McIlree, EPRI Assessment Manager
Electric Power Research Institute
P. O. Box 10412
3412 Hillview Ave.
Palo Alto, CA 94303

Frank Ammirato, EPRI
Inspection Manager
EPRI NDE Center
P. O. Box 217097
1300 W. T. Harris Blvd.
Charlotte, NC 28221

Gary D. Moffatt, Technical Chair
Repair/Mitigation Task
V. C. Summer Nuclear Station
P. O. Box 88
Jenkinsville, SC 29065

Mr. Jack Bailey, Chair
Materials Reliability Program
1101 Market Street - LP 6A
Chattanooga, TN 37402

Larry Mathews, MRP
Southern Nuclear Operating Company
Manager, Inspection and Testing Services
P. O. Box 1295
Birmingham, AL 35201

Vaughn Wagoner, Technical Chair
Assessment Committee
Carolina Power & Light Company
One Hannover Square 9C1
P.O. Box 1551
Raleigh, NC 27612

C. Thomas Alley, Jr., Technical Chair
Inspection Task
Duke Power Company
Nuclear General Office
526 South Church Street
Mail Code EC090
PO Box 1006
Charlotte NC 28201

U.S. NUCLEAR REGULATORY COMMISSION

**PRELIMINARY STAFF TECHNICAL ASSESSMENT FOR
PRESSURIZED WATER REACTOR VESSEL HEAD PENETRATION NOZZLES
ASSOCIATED WITH NRC BULLETIN 2001-01, "CIRCUMFERENTIAL CRACKING OF
REACTOR PRESSURE VESSEL HEAD PENETRATION NOZZLES"**

NOVEMBER 2001

(PROPRIETARY DESIGNATION REMOVED DECEMBER 4, 2001)

|

CONTENTS

| | | |
|---------|--|----|
| 1.0 | INTRODUCTION | 1 |
| 2.0 | CRACK INITIATION | 2 |
| 2.1 | Environment in CRDM Annulus Region | 2 |
| 2.1.1 | Staff Conclusions | 4 |
| 2.2 | Ranking and Activation Energies | 5 |
| 2.2.1 | Phenomenological and Statistical Initiation Models | 6 |
| 2.2.2 | Staff Conclusions | 11 |
| 3.0 | CRACK GROWTH RATE | 11 |
| 3.1 | Staff Conclusions | 15 |
| 4.0 | STRESS ANALYSIS AND CRACK-DRIVING FORCE | 15 |
| 4.1 | Past Babcock & Wilcox (B&W) Owners Group Efforts | 16 |
| 4.2 | On-Going Industry Efforts | 17 |
| 4.2.1 | Stress Analyses | 17 |
| 4.2.1.1 | Pressure Stresses | 17 |
| 4.2.1.2 | Residual Stresses | 17 |
| 4.2.1.3 | Thermal Expansion Differences | 19 |
| 4.2.1.4 | Cyclic Thermal Stresses | 19 |
| 4.2.2 | Crack-Driving Force Analyses | 19 |
| 4.3 | On-Going NRC-Funded Efforts | 20 |
| 4.4 | Staff Conclusions | 22 |
| 5.0 | CRITICAL CRACK SIZE | 24 |
| 5.1 | Staff Conclusions | 25 |
| 6.0 | DETERMINISTIC ASSESSMENT | 26 |
| 6.1 | Introduction | 26 |
| 6.2 | Base Case | 26 |
| 6.2.1 | Assumed Critical Flaw Size | 27 |
| 6.2.2 | Assumed Crack Growth Rate | 28 |
| 6.2.3 | Assumed Initial Flaw Size | 28 |
| 6.2.4 | Base Case Results | 30 |
| 6.3 | Uncertainties and Sensitivity Studies | 31 |
| 6.4 | Conclusions from Deterministic Calculations | 37 |
| 7.0 | PROBABILISTIC ASSESSMENT | 37 |
| 8.0 | INSPECTION TIMING | 38 |
| 9.0 | REFERENCES | 41 |

1.0 INTRODUCTION

From the experience at Oconee Nuclear Station Units 1 and 3 (ONS-1 and ONS-3), two distinct chronologies were identified as sources for circumferential cracking on the outside diameter (OD) of the control rod drive mechanism (CRDM) nozzles. In one case, an axial crack could initiate due to primary water stress corrosion cracking (PWSCC) and grow in the interface between the nozzle base material and the J-groove weld. This crack could progress along the interface until it reaches a location above the J-groove weld, producing a through-wall crack and resulting in leakage of primary coolant into the annulus between the nozzle and the reactor pressure vessel (RPV) head. At this location, the stress levels in the nozzle could produce a turning of the axial crack such that the crack could begin to propagate in a circumferential orientation along the profile of the weld.

In the second case, an axial crack in the nozzle or a crack in the J-groove weld could initiate and propagate to the point that a through-wall crack would permit leakage of primary coolant into the annulus between the nozzle and the RPV head. As leakage from this crack occurs, an environment conducive to the initiation of stress corrosion cracking (SCC) could be produced in the annulus. After some characteristic initiation time period, a crack or a series of cracks could initiate on the OD of the nozzle in the circumferential orientation along the J-groove weld profile at a region of high axial tensile stress on the nozzle. This crack or series of cracks could propagate in the nozzle in the same orientation along the J-groove weld profile. A series of cracks could ultimately link up to form a larger crack.

A comprehensive analysis of circumferential cracking in vessel head penetration (VHP) nozzles would require treatment of the following aspects of the issue:

- a. the time to initiate a crack on the inside diameter (ID) of the nozzle or in the J-groove weld,
- b. the crack growth rate (da/dt) for the nozzle base material or the J-groove weld in a primary water environment, and determination of the time for the crack to grow through-wall (allowing primary water leakage into the annulus),
- c. the time to begin circumferential cracking on the OD of the nozzle, including the time to establish a conducive environment in the annulus and initiate independent circumferential crack(s), or the time for an axial crack to turn and begin propagating in the circumferential direction along the weld profile,
- d. the crack growth rate (da/dt) for the circumferential crack on the nozzle OD in the annulus environment set-up by the leaking coolant, including consideration of whether this environment is static or time dependent, evaluation of the time for the crack to grow through-wall or propagate as a part-through wall crack, and determination of the time for the crack to grow to reach the critical flaw size, and
- e. the critical flaw size, based on tensile overload of the remaining ligament of the nozzle, including consideration of safety margins such as the American Society of Mechanical Engineers (ASME) Code margin of three on pressure loads.

Included in this comprehensive analysis at various points could be definition of inspection activities that would be sufficient to effectively manage the cracking through detection, characterization and remediation of defects, and assessment of the impact of these inspection activities on the population of flaws in the nozzles.

This assessment provides a discussion of the state of knowledge for each of the above variables and a model that integrates the variables to support analysis of the VHP nozzle cracking phenomena. A few important points need to be made:

- 1) For some of the variables the existing data are sparse or in some cases nonexistent, thus
- 2) the data and models for assessing this phenomena are still under development.
- 3) This assessment represents the staff's best understanding of the technical aspects of the issue at this time, and
- 4) additional work needs to be done by the industry to provide a better technical understanding and basis to support a program for effective management of this degradation mechanism.

Section 2 of this assessment summarizes the existing data for crack initiation time in Alloy 600 base metal and Alloy 182 weld metal under primary water conditions (and in Alloy 600 base metal under postulated annulus environmental condition), Section 3 summarizes the available crack growth rate data for the materials and environments of interest, Section 4 describes the stress state in the penetration nozzles (including residual and operating stresses), and Section 5 describes the critical crack size for circumferential cracks, considering both failure of the nozzle and a safety margin of three on the pressure load.

2.0 CRACK INITIATION

2.1 Environment in CRDM Annulus Region

Crack initiation times and crack growth rates are dependent on the environment. Either a caustic or an acidic environment can decrease crack initiation times and increase crack growth rates. Therefore, it is very important to understand the environment in which cracking will occur in VHP nozzles since it will influence the assumed crack initiation and growth rates used in cracking assessments such as that described below.

For cracking to initiate on the outer surface of a VHP nozzle, the surface must be exposed to a conducive environment. This environment can be established when cracks initiate and propagate through either the Alloy 182 J-groove weld or through the nozzle base metal. From experience at ONS-1 and ONS-3, leak rates through the cracks in the J-groove welds can be very small, $\ll 0.004$ liters per minute (0.001 gallons per minute, gpm). The potential leak rate through cracks in the nozzle base metal could potentially be much larger, but experience shows that even in the case of cracks as large as those observed at ONS-3, the amount of boric acid deposited on the head indicates that the leak rates were very small, with a 165° through-wall circumferential crack depositing less than 16 cm^3 (1 in.^3) of boric acid on the RPV head in one year. The amount of boric acid deposit associated with this flaw was ~ 10 grams (0.02 lbs),

equivalent to an effective leak rate of 6×10^{-6} liters per minute (1.5×10^{-6} gpm), based upon a 0.004 liters per minute (0.001 gpm) leak depositing about 7 kg (15 lbs) of boric acid in a year. Although the VHP nozzles are typically manufactured with interference fits, finite element analyses show that gaps on the order of 0.03 to 0.05 mm (0.001 to 0.002 inches) are expected to open during operation (depending on the initial interference fit), although in some cases the interference fits could remain even at operating temperatures. The resulting flow paths through the annulus between the VHP nozzle and the RPV head are very large compared to the flow paths through the PWSCC cracks in the Alloy 182 J-groove welds that join the nozzle to the vessel. This comparison suggests that unless the annulus becomes blocked, the leaks would vent and the annulus would not see a steam or water environment that would promote cracking above the weld. However, at least initially there will be a very large pressure drop through the through-wall crack in either the J-groove weld or the nozzle itself, and since the temperature will still be about 300°C (572°F), the water will flash to steam, and boric acid will deposit in the annulus. Also, at least initially, the annulus with an open gap should be accessible to the containment air. In this case any moisture as steam or water in the annulus will produce general corrosion of the low alloy steel vessel. It is not until a sufficient blockage of corrosion products associated with corrosion of the low alloy steel occurs that a steam or water environment would be available to produce SCC on the OD of the VHP nozzle.

Because the process of flashing the leaking primary coolant to steam provides a mechanism to concentrate species from the primary water, fluid in the annulus region could be a much more concentrated chemical solution than the primary coolant. The actual composition of the annulus solution would depend on the corrosion reactions with the low alloy steel, the transport processes through the deposits, the relative volatilities of lithium hydroxide and boric acid, and the impurities present in the primary coolant. The variability in the degree of blockage due to interference fits or corrosion deposits means that the boiling transition can occur anywhere along the leak path. Thus the environment immediately above the J-groove weld during a leak event can be:

- superheated steam if the pressure drop to the saturated vapor pressure occurs within the stress corrosion crack, or
- boiling and consequently concentrated pressurized water reactor (PWR) primary water if boiling occurs at the exit of the stress corrosion crack, or
- normal PWR primary water when the boiling transition is well above the J-weld (Ref. 1).

Although the annulus is nominally open to the containment atmosphere, it is very unlikely that the root of the annulus near the J-groove weld is oxygenated. Diffusion models suggest that back diffusion of oxygen into the annulus environment cannot occur except at very low mass flow rates. Secondly, a narrow annulus (and crack) would be de-oxygenated due to consumption of any incoming oxygen by general corrosion on the annulus walls very near the mouth.

Because hydrogen diffuses readily through steel at temperatures of ~300°C (572°F) from PWR primary water to the outside of the pressure vessel, the hydrogen fugacity in the annulus will be close to the primary water hydrogen overpressure. This should be sufficient to maintain the corrosion potential close to that of the Ni/NiO equilibrium. Consequently, stress corrosion

susceptibility of Alloy 600 is very similar in both situations at the same temperature. Even if the concentration of hydrogen is depleted by local boiling, electrochemical coupling between the low alloy steel and the Alloy 600 nozzle would likely lower the corrosion potential of the Alloy 600 nozzle into the same range as the normal hydrogen partial pressure of PWR primary water.

As PWR primary water flashes to steam, lithium hydroxide and boric acid can concentrate near the liquid/vapor interface. Despite the volatility of boric acid relative to lithium hydroxide, MULTEQ calculations at a constant temperature of 313°C (595°F) and a constant mass flow rate suggest that these components will concentrate until lithium metaborate, LiBO_2 , precipitates (Ref. 1). At this point, the estimated increase in the pH is 8 to 8.6. This is significantly higher than 6.8 to 7.4 of normal PWR primary water but not particularly "caustic."

At very low leak rates, boiling can occur very rapidly with no mixing with any remaining liquid within the annulus. In this case, MULTEQ, with lithium metaborate again as the precipitating species, predicts that the environment evolves initially in the alkaline direction to a maximum pH of 7.8 and then in the acidic direction to a pH of 4.5 (Ref. 1). Note that neutral water at the same temperature of 313°C (595°F) has a pH of 5. Chemical and electrochemical reactions with the metal components of the annulus are not included in the MULTEQ calculations. The annulus condition involves a small volume of water and a very large surface area of Alloy 600 on one side of the annulus and low alloy steel on the other. Boric acid solutions at ~300°C (572°F) react fairly rapidly with low alloy steel to produce insoluble borates and the pH is consequently buffered at near neutral values by iron hydroxide in solution. A modified MULTEQ calculation incorporating iron metaborate as a possible solid precipitate in boiling PWR primary water has shown that its very low solubility ensures that the pH does not shift significantly in the acid direction (Ref. 1).

Even these modest pH shifts may overestimate the changes that actually occur. Studies of deposits on PWR fuel pins that are responsible for the "Axial Offset Anomaly" suggest that boron is precipitated not as lithium metaborate but as nickel boroferrite, Ni_2FeBO_5 . Nickel boroferrite is very likely to be much less soluble in water than lithium metaborate, or even iron metaborate, and to incorporate lithium readily into its crystal structure, but it does not yet appear in the thermodynamic database of MULTEQ. Such a low solubility would severely limit the possible movement of pH relative to normal PWR primary water (Ref. 1).

The work of Berge et al. (Ref. 2) suggests that in the absence of oxygen and other impurities such as chlorides, a concentrated boric acid solution is not detrimental to Alloy 600, although even low levels of dissolved oxygen and chlorides can greatly increase susceptibility. The susceptibility of Alloy 600 is very sensitive to the presence of acidic or strongly basic environments as shown in Figure 1 (Ref. 3), but the pH ranges expected in a VHP annulus with leakage from the primary side appear unlikely to result in susceptibilities more than a factor of two higher than those observed in PWR primary water.

2.1.1 Staff Conclusions

Based on the preceding discussion, the environment in the annulus is not expected to be highly aggressive, and thus the staff has used crack initiation times and crack growth rates associated with normal PWR reactor coolant chemistry in its assessment. However, it is important that annulus deposits from a leaking nozzle be obtained and analyzed to provide confirmation of the assumed annulus environment.

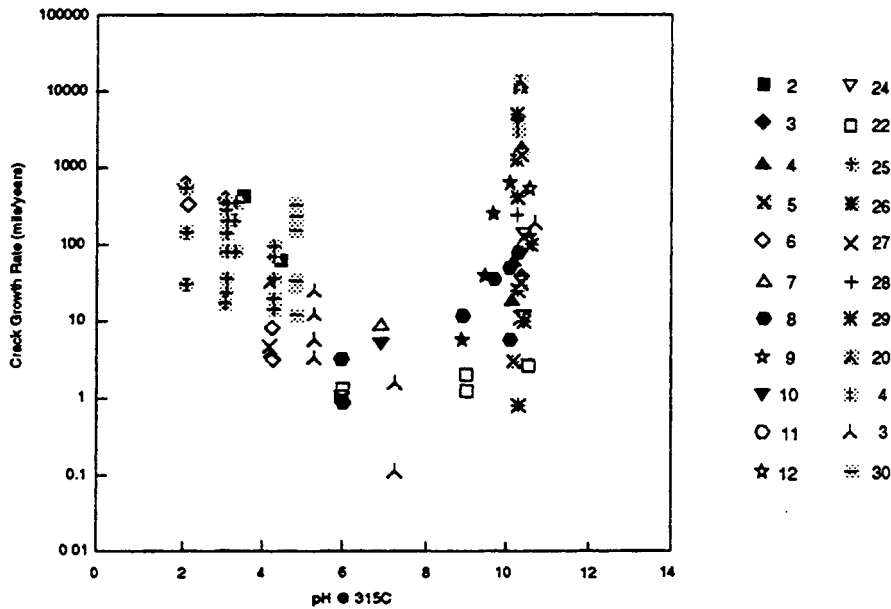


Figure 1 Dependence of crack growth rate in Alloy 600 on pH (Ref. 3).

2.2 Ranking and Activation Energies

PWSSC of Alloys 600 and 182 is strongly dependent on the characteristics of the operating environment (e.g., applied stress, temperature, operating time, and chemistry of the environment) and the material (e.g., microstructure, cold work, yield strength). A substantial amount of information is available to characterize the susceptibility of Alloy 600 and a variety of schemes for susceptibility indexing have been proposed (Refs. 4 to 7), with the latest susceptibility model proposed by the Materials Reliability Project (MRP) in Ref. 8. The material characteristics of most direct interest are the nature of the carbide precipitates and the degree of cold work. Carbon precipitates can form either on grain boundaries or they can be intragranular. A nearly continuous distribution of carbides on the grain boundaries with little intragranular precipitation of carbides is the most resistant microstructure. The nature of the grain boundary carbide distribution is often described in terms of percentage of grain boundary coverage or decoration (GBD). Cold work also significantly increases the susceptibility of Alloy 600 to PWSSC.

For cracking of VHP nozzles, little is known about the detailed characterization of the plant-specific materials of interest and susceptibility rankings must be determined primarily on the basis of operating conditions (e.g., temperature and operating time). The effect of temperature on PWSSC initiation and growth can be described in terms of activation energies. The available work on the activation energy of Alloy 600 has been reviewed by Smilowska and Rebak (Ref. 9) and Majumdar (Ref. 10). For crack initiation, the value of the activation energy is generally found to be 40 to 50 kcal/mole (167 to 209 kJ/mole). The activation energy for crack growth is generally taken as 30 to 35 kcal/mole (125 to 146 kJ/mole). Although the median life does show a well defined Arrhenius-type behavior, the initiation time for individual specimens is statistically distributed. Figures 2a and 2b show data by Webb (Ref. 11) for the determination of an activation energy, in this case 50.6 kcal/mole (212 kJ/mole) with a standard

error of 3.8 kcal/mole (16 kJ/mole), and the distribution of initiation times for individual specimens. As would be expected, much more scatter is observed when one attempts to correlate field data, as illustrated in Figure 3. The lines in Figure 3 correspond to an activation energy of about 40 kcal/mole (167 kJ/mole). Fewer data are available for Alloy 182, but it is reasonable to expect that the activation energies are similar (Ref. 11). Since the limiting process in VHP nozzle cracking is expected to be the initiation of the cracks and not crack growth, the appropriate activation energy to characterize VHP nozzle cracking is 40 to 50 kcal/mole (167 to 209 kJ/mole) as proposed by the MRP (Ref. 8).

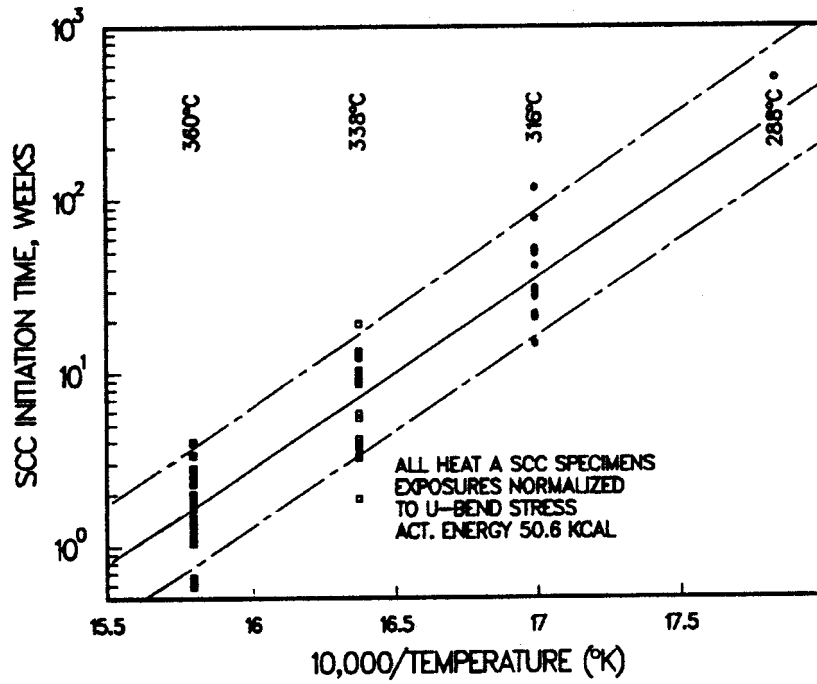
2.2.1 Phenomenological and Statistical Initiation Models

The median failure time (Θ_m) depends on the applied stress (σ) as well as the temperature (T). Webb fit his data on median failure times with an equation of the form:

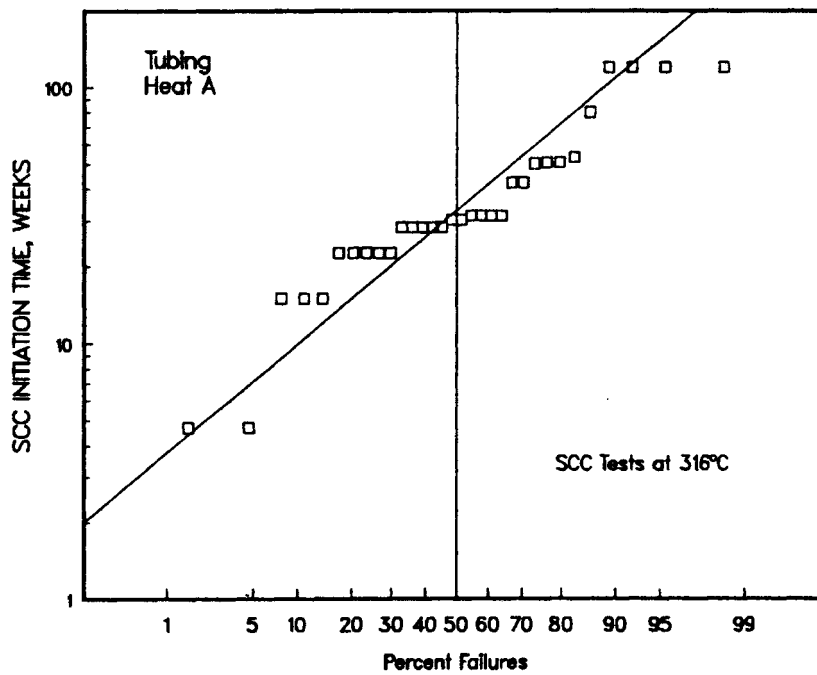
$$\Theta_m = A \sigma^{-m} e^{-Q/RT} \quad (1)$$

where the stress exponent m is 5.7, Q is the activation energy, and R is the universal gas constant, 1.987 cal/mol-°K (8.314 J/mol-°K). Other investigators have proposed similar relations with stress exponents on the order of 4 (Refs. 6 and 12). The most significant stresses acting on the weld are the residual stresses due to welding, but additional sources would be installation stresses associated with activities such as straightening of the nozzles during installation. Although the welding residual stresses would be dependent on welding process, it is likely that this distribution would not vary too much from unit to unit, assuming that the same welding sequencing was consistently used. More variation might be expected in microstructure, which would affect the pre-exponential term A in the expression for Θ_m . Data may be available to characterize the carbon level in the weld metal, which could provide an additional ranking parameter, but because of the relatively strong dependence of the median failure time on temperature, the proposal of the MRP (Ref. 8) to rank units in terms of susceptibility based on operating temperature is reasonable, due to the lack of material specific information available, and the use of an appropriate activation energy value (Ref. 8). However, the resulting relative susceptibility should not be used to infer that cracking will necessarily occur at plants in the sequence provided by the ranking. The variation in parameters such as microstructure and stresses could result in a plant initiating cracking at an earlier time than a plant with a higher susceptibility ranking.

The ranking is in terms of the median failure time. Figure 4 shows a comparison of the failure distribution data for Alloy 600 and Alloy 182 obtained by Webb (Ref. 11). The median time to failure is greater for Alloy 182 than for Alloy 600 and the slope of the failure distribution curve is flatter for Alloy 600 than for Alloy 182. A flatter slope indicates that failure times are more tightly grouped about the median. A steeper slope indicates a wide scatter in failure times, i.e., the failure distributions have long tails.



(a)



(b)

Figure 2 For Alloy 600 (Ref. 11): (a) Initiation time as a function of inverse temperature; (b) Distribution of initiation times for individual specimens under a fixed set of conditions.

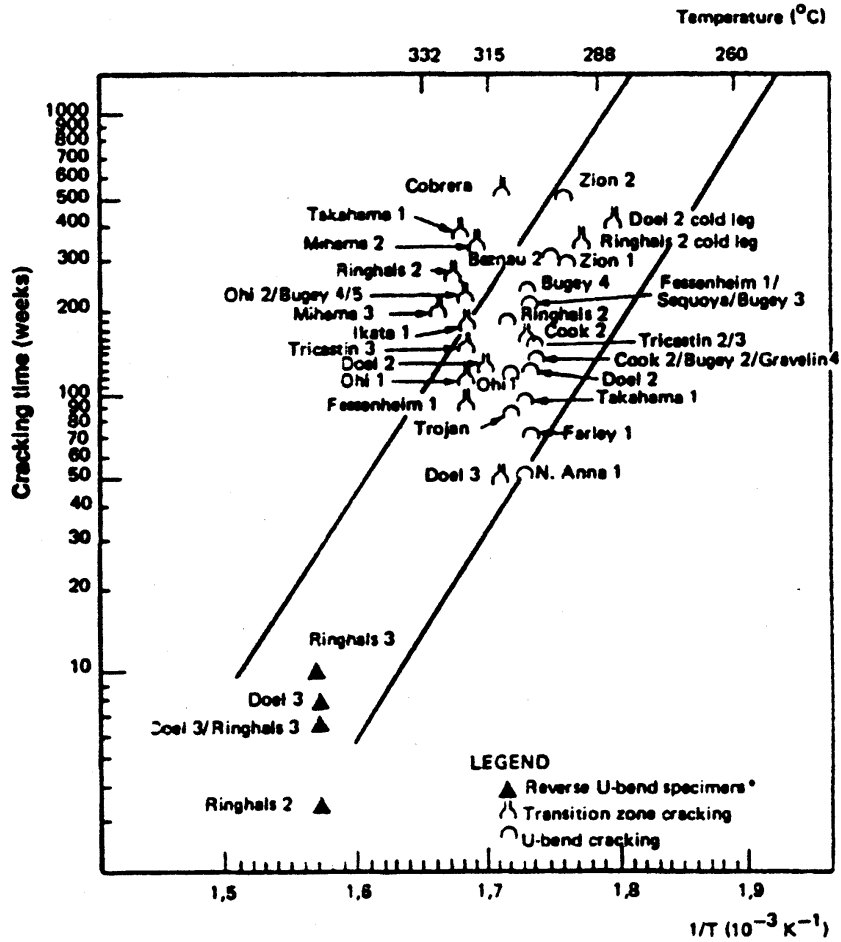


Figure 3 Dependence of initiation time on inverse temperature for field cracking.

Instead of determining the median time to failure through a phenomenological model such as Eq. (1), Staelhe, Gorman and their coworkers have popularized the use of statistical analysis of actual in-reactor failure data to describe the initiation of SCC cracks (Refs. 13 and 14). Although both lognormal and Weibull distributions have been examined, the Weibull distribution is more flexible and has been more generally used (Refs. 6, 13 and 14). The Weibull probability density and cumulative probability functions are given by:

$$\begin{aligned}
 p(t) &= \frac{b}{\theta} \left(\frac{x}{\theta} \right)^{b-1} \exp \left[- \left(\frac{x}{\theta} \right)^b \right] \\
 F(t) &= 1 - \exp \left[- \left(\frac{x}{\theta} \right)^b \right]
 \end{aligned}
 \tag{2}$$

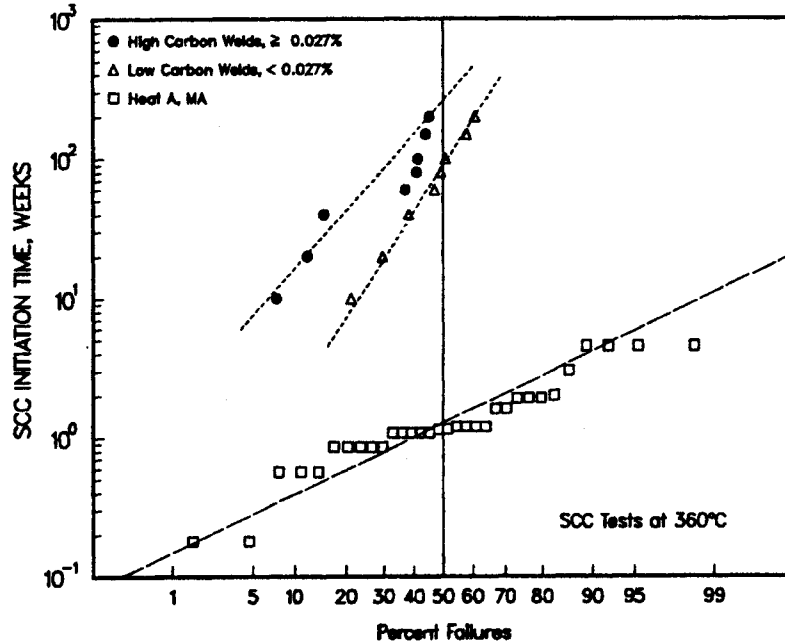


Figure 4 Distribution of failure times for Alloy 182 welds and Alloy 600 (Ref. 11).

For a given value of the slope b , the corresponding Weibull scale parameters can be calculated from the inspection results at each plant. Because only a limited amount of data from a single inspection is available, values of the Weibull slope b must be assumed on the basis of laboratory and previous related plant experience. Results for plant and laboratory data in Appendix C of Staelhe et al. (Ref. 13) show that b can have values ranging from 1 to 6.4, as shown in Figure 5. The median value of b from Figure 5 is 1.4. Scott's analysis of CRDM cracking in France was based on a value of 1.5 (Ref. 6). Lower values of b lead to higher probabilities of failure because they imply a wider scatter of initiation times so that, for a given observation of cracking, the probability of early crack initiation increases with decreasing b . The MRP work (Ref. 15) used a value of 3 for b . This value does not appear to be representative of the data in Figure 5.

The scale parameter Θ can then be calculated from the observed failure fraction F at time T :

$$\theta = T \left[\ln \left(\frac{1}{1-F} \right) \right]^{-\frac{1}{b}} \quad (3)$$

where the observed failure fraction is the median rank value, i.e, the observed fraction multiplied by

$$\frac{i - 0.3}{n + 0.4} \quad (4)$$

where i is the rank order number and n the sample size. Using a value of 1.5 for b , Table 1 shows values of Θ for the seven plants that have reported cracking during their fall 2000 to fall 2001 inspections.

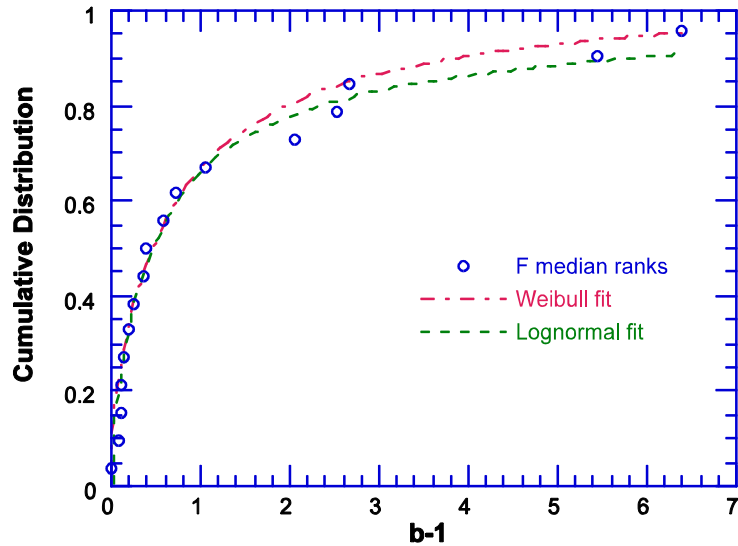


Figure 5 Distribution of the Weibull slope b for cracking of steam generator tubes. By expressing the results in terms of $b-1$ the results can be fit by Weibull or lognormal distributions.

To estimate the range of possible scale factors in the population of plants, it was assumed that for a given value of the Weibull slope, the values of the scale parameter follow a lognormal distribution and the values from the seven plants that have reported cracking during their fall 2000 to fall 2001 inspections were used to estimate the lognormal parameters (Table 1).

Table 1 Values of the Weibull Scale Parameter Based on Inspection Results for a Weibull Slope $b = 1.5$

| Plant | Number of Leaking Nozzles | Actual EFPY | EFPY @ 315°C (600°F) | Θ |
|----------------------|---------------------------|-------------|----------------------|----------|
| Oconee Unit 3 | 9 | 20.1 | 21.7 | 82.9 |
| Oconee Unit 2 | 4 | 20.3 | 22.0 | 152.5 |
| Oconee Unit 1 | 1 | 20.4 | 21.7 | 463.3 |
| ANO Unit 1 | 1 | 18.0 | 19.5 | 416.3 |
| TMI Unit 1 | 3* | 16.8 | 17.5 | 150.4 |
| Crystal River Unit 3 | 1 | 14.9 | 15.6 | 333.0 |
| Surry Unit 1 | 2* | 19.5 | 16.6 | 146.4 |

Note: EFPY values are as of February 2001.

* Preliminary information.

The expected fraction of CRDM nozzles that will have developed leaks can be estimated by a Monte Carlo analysis over the estimated distributions for Θ . The expected fractions of nozzles that are expected to leak in terms of EFPY at 315°C (600°F) are shown in Table 2. The Arrhenius relationship can be used to extrapolate to other operating temperatures using an activation energy for initiation of 40 to 50 kcal/mole (167 to 209 kJ/mole). Although the expected number of leaks is about 2 for a plant with 69 VHP nozzles, the number can vary.

Table 2 Fraction of CRDM Nozzles with Cracks as a Function of EFPY at 315°C (600°F)

| EFPY | 5 th percentile | Median | 95 th percentile |
|------|----------------------------|-------------|-----------------------------|
| 15 | 0.004 | 0.019 | 0.090 |
| 20 | 0.006 (0.4) ^a | 0.029 (2.0) | 0.135 (9.3) |
| 25 | 0.008 | 0.040 | 0.184 |

^a Expected number of leaks for plants with 69 nozzles

2.2.2 Staff Conclusions

The operating experience of leaking nozzles, based on data available as of November 1, 2001, appears to be well modeled by the Weibull analysis with $b = 1.5$. The operating experience appears to fit between the 5th percentile to the 95th percentile. Note that final results for two of the plants and the results of additional inspections will be used to update this analysis.

3.0 CRACK GROWTH RATE

A wide range of crack growth rates (CGR) has been reported for Alloy 600 in primary coolant environments. Comprehensive reviews are given in Refs. 8, 9, and 16. Figure 6 from Ref. 16 summarizes much of the available data for a variety of product forms and shows correlations for the crack growth rate based on the work of Scott (Ref. 17). The results in Figure 6 have been normalized to a temperature of 330°C (626°F). For lower temperatures the crack growth rate can be reduced using an activation energy of 31 kcal/mole (130 kJ/mole) according to Ref. 16. The lower correlation is typically suggested for materials which are not cold worked, while the upper curve is proposed as appropriate for materials (like steam generator tubing) that contain cold work. The upper curve gives roughly a limiting crack growth rate of 30 mm/yr (1.2 in./yr).

In Figure 7, the curves have been replotted showing only data obtained on product forms expected to be representative of CRDM nozzle materials (Refs. 18 to 23). There appears to be a strong dependence of the crack growth rate on the particular heat of material. One heat used in tests by Cassagne et al. (Ref. 20) appears to have very high growth rates. This same heat was tested by three different organizations, which all reported high growth rates for this material (Ref. 21). This heat does have a low degree of grain boundary carbide coverage, but Foster et al. could not identify a strong effect of grain boundary carbide coverage on crack growth rate (Ref. 18). The data of Lidar et al. (Ref. 23) is also of particular interest. They studied the effect

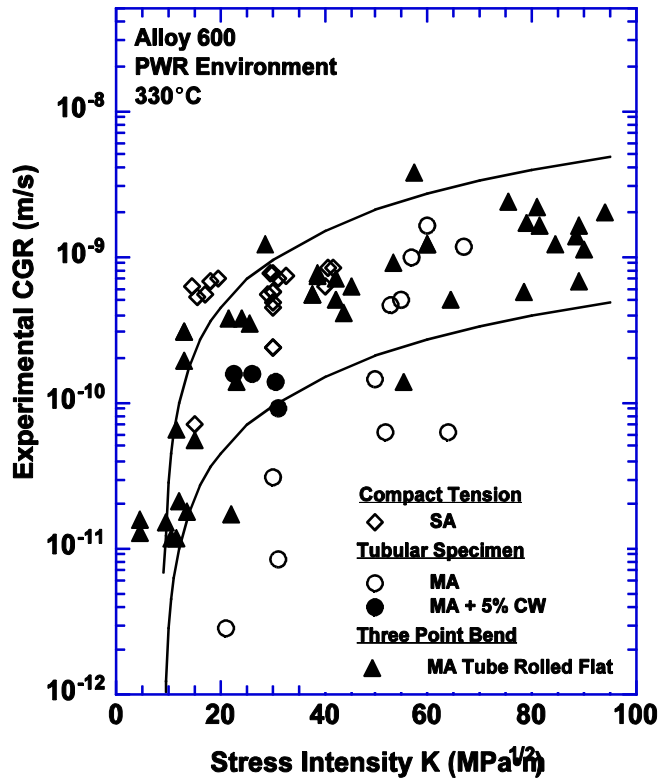


Figure 6 Crack growth rates in PWR environments for a variety of product forms. The curves correspond to a correlation based on the work of Scott (Ref. 17).

of a range of Li, boric acid, and H₂ levels on the crack growth rate and found that relatively small variations in the water chemistry appeared to produce surprisingly large changes in crack growth rate. These results suggest that the crack growth rate correlation used in previous safety analyses of CRDM cracking (the lower curves in Figures 6 and 7) may underestimate the growth rate for a significant number of heats of Alloy 600 used for nozzle penetrations.

The data for the different heats of nozzle material can be fit using the Scott correlation given by:

$$\frac{da}{dt} = A (K-9)^{1.16}$$

where a value of A can be determined for each heat of material from the measured CGR data. Foster et al. found no systematic variation of A with a variety of metallurgical parameters such as grain boundary carbide coverage, yield stress, etc. (Ref. 18). As shown in Figure 8, the values of A for the different heats are reasonably well represented in terms of a lognormal distribution with a log mean of -26.48 and a log standard deviation of 1.06. The values of 2.8×10^{-11} and 2.8×10^{-12} corresponding to the upper and lower curves respectively in Figures 6 and 7 represent the 97th and 37th percentiles of the distribution.

Percentile values of A that bound a given fraction of the available heats at a given confidence level can be determined from the distribution. Several pertinent values are given in Table 3.

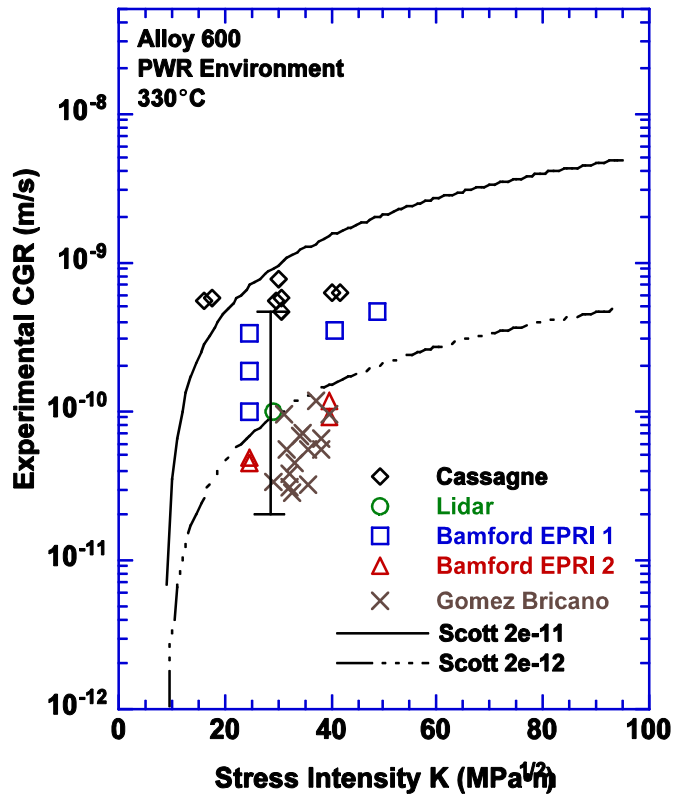


Figure 7 Crack growth rates in PWR environments for vessel head penetration materials. The curves correspond to a correlation based on the work of Scott (Ref. 17). The vertical bar associated with data of Lidar et al. (Ref. 23) denotes the range of growth rates they observed over a range of water chemistries.

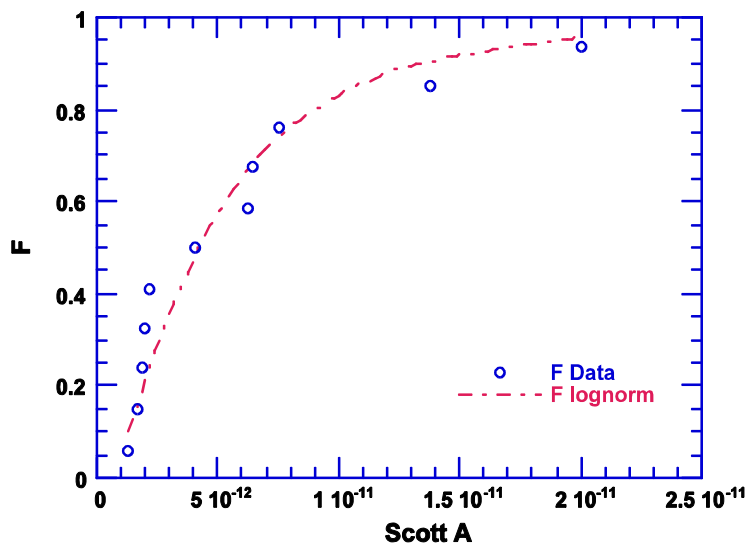


Figure 8 Cumulative distribution of the parameter A in the Scott CGR correlation for heats of nozzle materials studied by Foster et al. (Ref. 18), Cassagne et al. (Ref. 20), and Gómez Briceño and Lapeña (Ref. 22).

Table 3 Values of the Scott CGR Parameter A for Alloy 600 at 325°C (617°F) as a Function of the Percentage of the Population Bounded and the Confidence Level

| Confidence Level | Population Percentage | | | |
|------------------|-----------------------|-----------------------|-----------------------|-----------------------|
| | 95 | 90 | 67 | 50 |
| 50 | 1.8×10^{-11} | 1.2×10^{-11} | 5.1×10^{-12} | 3.1×10^{-12} |
| 67 | 2.3×10^{-11} | 1.5×10^{-11} | 5.8×10^{-12} | 3.5×10^{-12} |
| 90 | 4.2×10^{-11} | 2.4×10^{-11} | 7.5×10^{-12} | 4.4×10^{-12} |
| 95 | 5.6×10^{-11} | 3.1×10^{-11} | 8.4×10^{-12} | 4.8×10^{-12} |

The 95/50, 90/50, etc. are “best estimate” values in the sense that the true 95th, 90th, etc. percentiles have an equal likelihood to be less than or greater than these values. In Figure 9, the 95/50 and 50/50 curves are compared with French data (Ref. 21) on crack growth rates observed in the field.

The field measurements are based on ultrasonic measurements of crack depth. The K values are based on calculated values of residual stresses. As such they are subject to large uncertainties (error bars have been estimated but not shown because they obscure the figure). However, although an individual data point is subject to large uncertainties, the overall trends indicated by the data are interesting. The 95/50 curve developed from the laboratory data bounds most of the data, as expected. Most of the data, however, lies above the 50/50 curve. This is not too surprising. Susceptibility is highly variable from heat to heat and cracking in the field tends to occur in the most susceptible heats. One implication of these results is that calculations of the conditional probability of failure of cracks (conditional on the existence of the cracks) should not be calculated based on the complete distribution shown in Figure 8, but only on the portion corresponding to a cumulative probability greater than 0.5.

Electricite de France (EDF) does not recommend the use of the Scott model to describe CGRs in Alloy 600 (Ref. 21). They use a model with $(K-9)^{0.1}$, which for all practical purpose gives plateau-like behavior for $K > 9 \text{ MPa}\sqrt{\text{m}}$ ($8.2 \text{ ksi}\sqrt{\text{in.}}$). The plateau CGR in this case is about $7 \times 10^{-10} \text{ m/s}$ ($2.8 \times 10^{-9} \text{ in/s}$). Such an assumption is consistent with the data shown in Figure 9, but this data could also be interpreted viewing the few data points at high K as representative of heats that just happen to have lower CGR curves. Further, it is very difficult to deduce K dependence when the data represents a mixture of heats (the field data probably include tens of heats). Laboratory tests under load control generally follow a K dependence similar to that predicted by the Scott model, but because the specimens lose constraint, no valid laboratory data appear available for $K > 40 \text{ to } 50 \text{ MPa}\sqrt{\text{m}}$ ($36 \text{ to } 45 \text{ ksi}\sqrt{\text{in.}}$). The highest laboratory CGR data are about $7 \times 10^{-10} \text{ m/s}$ ($2.8 \times 10^{-9} \text{ in/s}$), similar to the EDF bound.

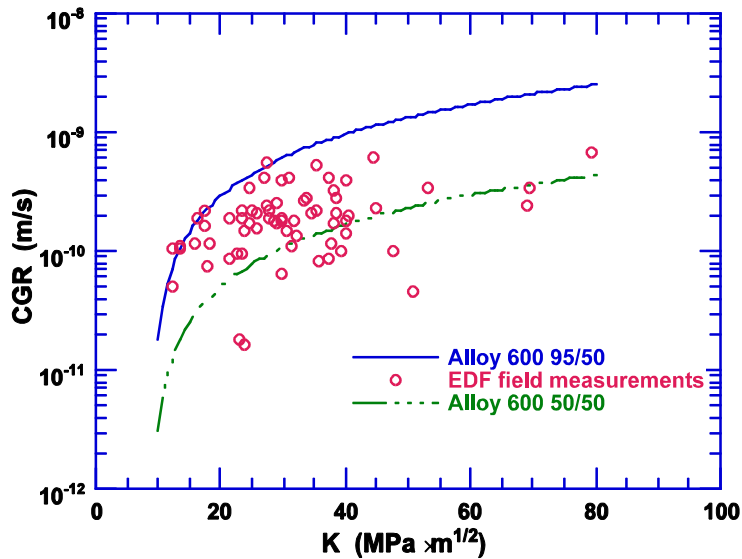


Figure 9 EDF field measurements of CGRs compared with 95/50 and 50/50 CGR curves developed from laboratory data (Ref. 21).

Although the data reviewed here were developed in a primary coolant environment, they are felt to be applicable to the discussion of the growth of cracks in a VHP nozzle. As discussed in Section 2.1, the environment in the annulus may well be a more concentrated solution than the primary coolant, but it is unlikely to have a pH in a range that would lead to significantly accelerated cracking and it is unlikely to be oxygenated. Even if the annulus environment is more aggressive than expected based on the arguments in Section 2, once a through-wall crack has grown to any significant extent, the crack opening area will be large enough such that the primary coolant is now able to communicate with the fluid in the annulus at least by diffusion. Because the volume of the fluid in the annulus is very small, the environment should be controlled by the primary coolant chemistry.

The growth rates discussed in this section are used in conjunction with the applied stresses and crack driving forces in Section 4.2, which follows, to support the deterministic assessment in Section 8.

3.1 Staff Conclusions

The staff concludes that the crack growth rate data for PWSCC is a reasonable approximation for OD VHP nozzle cracking, based on the data and analyses in this section. The staff has concluded that the crack growth rate function values given in Table 3 are appropriate for use at 325°C (617°F).

4.0 STRESS ANALYSIS AND CRACK-DRIVING FORCE

Stress analysis and crack-driving force analyses have been funded in the past by several international utilities, vendors, and regulatory agencies, as well as by several U.S. owners groups and the Electric Power Research Institute (EPRI). A short review of some of the pertinent Babcock & Wilcox (B&W) Owners Group past efforts are first given in this section. Secondly, on-going industry efforts at Structural Integrity Associates (SIA) and Dominion

Engineering (coordinated through EPRI and augmented by individual U.S. utilities) are summarized. Finally initial NRC-funded efforts are also summarized at the end of this section.

4.1 Past Babcock & Wilcox (B&W) Owners Group Efforts

Some of the earlier relevant CRDM analysis efforts conducted by U.S. industry were performed by B&W. Reference 24 describes those efforts on analysis of an external circumferential crack immediately above the J-groove weld in a CRDM nozzle subjected to service loading conditions. The analysis was focused on a small initial circumferential surface crack of 0.025 mm (1 mil) depth located on the external surface of the nozzle, at the top of the weld zone and on the downhill side of the nozzle. Stress solutions (taken from Ref. 25) were generated from a 3-D finite-element model of an uncracked hillside CRDM nozzle inserted in a vessel head segment. The model incorporates a loading sequence extending from shop installation through service operating conditions, i.e., nozzle shrink fit, welding processes, hydrostatic testing, and steady-state operations. In Ref. 24, several observations were made concerning the axial loading of the near-weld region where the initial crack is positioned:

- The average stress around the nozzle was calculated to be relatively constant at approximately 138 MPa (20 ksi);
- The axial stresses mainly comprised secondary stresses resulting from welding processes and thermal loading;
- The remaining portion of the total axial stress was comprised of pressure-induced stresses, approximately 14 MPa (2 ksi) that were not significant compared to the residual welding and thermal stresses.

The crack growth analysis took the residual and thermal stresses as primary stresses and used the crack growth rate model developed by Scott (Ref. 26) from industry data for PWSCC of Alloy 600 steam generator tubing. Stress intensity factors were calculated by combining a cubic polynomial fit to the stress data with the linear-elastic fracture mechanics (LEFM) Raju-Newman solution (Ref. 27) for a circumferential surface crack. From these analyses, the report concluded that a minimum of six years was required for the crack to grow through the wall, assuming that all applied stresses were primary stresses. Reference 24 asserted it was unlikely that a circumferential crack would propagate through the wall and grow circumferentially along the nozzle-weld contour for the following reasons:

- More than 90 percent of the crack-driving force was due to residual stresses. A significant portion of those stresses would be relieved upon opening of the crack, thus arresting the crack at a point approximately 50-60 percent through the wall.
- Opening of a large through-wall crack would produce detectable leakage that provides ample warning prior to failure of the nozzle. The limit-load of the ligament was estimated to be less than 10 percent, which provided large margin for leakage to occur before failure was reached. Ovalization of the nozzle would produce sufficient paths to the exterior surface of the head to permit detection of a leak.
- The contact area between the ovalized nozzle and vessel head would be sufficient to resist any slippage.

Reference 24 observed that a 3-D finite element analysis incorporating crack growth with time would demonstrate the effects of stress relief associated with a circumferential crack propagating through the nozzle wall. The latter approach was not pursued because of the inordinate amount of computational effort required for such an analysis.

4.2 On-Going Industry Efforts

These results are primarily from the work of Dr. P. Riccardella of Structural Integrity Associates (SIA) in Ref. 28. The residual stress analyses were performed by Dominion Engineering and provided to SIA for their crack growth modeling work. The stress analysis aspects are first summarized, including the contributors to stress for CRDM nozzles, and then the crack-driving force for the deterministic assessment of circumferential cracking in Section 6 is described.

4.2.1 Stress Analyses

The contributing stresses to the potential for SCC cracking of CRDM nozzles are:

- Pressure stresses, including endcap loading on tube, and pressure loading on the crack faces (assuming no leakage for pressure drops through the crack),
- Weld residual stresses (perhaps the most significant stress component),
- Thermal expansion differences between the Alloy 600 tube and the RPV head low alloy steel, and
- Cyclic thermal stresses (from flow within the nozzle).

4.2.1.1 Pressure Stresses

The internal pressure in the upper head region of the vessel is relatively constant during operation, such that fatigue loading from pressure cycles need not be explicitly considered in the analysis. Once a crack initiates, the pressure stresses on the crack faces must be considered, especially for long cracks, as they can be a significant fraction of the axial stress on the crack. For ASME Code Section XI flaw evaluation procedures, a safety factor of three is typically used for pressure stresses.

4.2.1.2 Residual Stresses

Since the first occurrence of PWSCC in CRDM nozzles, the residual stresses resulting from welding in CRDM nozzles have been recognized as a major contributor to SCC. Analyses from the three PWR vendor owners groups placed emphasis on evaluation of the residual stresses. From the analyses at that time, cracking on the nozzle ID was expected to predominate over cracking on the nozzle OD due to higher stresses on the ID. In addition, cracking on the nozzle ID was expected to predominate in the axial orientation, due to higher hoop stresses than axial stresses (note that the crack plane orientation is perpendicular to the highest stresses). With the recent findings of circumferential cracking on the OD of nozzles above the J-groove welds preceded by through-wall cracking in the J-groove welds, the residual stress analyses have been reexamined by industry.

As described in Reference 28, experimental measurements of material removed from Ocone Unit 3 revealed a through-wall strength gradient, with the yield strength increasing from the inside surface of the nozzle to the outside surface. Accounting for this strength gradient results in higher residual stresses on the OD of the tube, compared with the traditional tube of uniform strength (which was also lower in strength when compared with the strength-gradient tube). Figure 10 illustrates the residual stress gradient (for typical operating temperature and pressures) for stresses in the longitudinal (axial) direction of the tube, as a function of through-wall thickness location and location around the circumference. These results show that the residual stresses vary from tension to compression as the location around the circumference changes from 0 to 180 degrees, with 0 degrees representing the uphill side of the nozzle (e.g., the side closest to the top of the head.) The trend of residual stress distribution through the thickness changes as the location around the circumference changes, indicating preferred crack initiation and growth locations.

For a crack that would initiate on the uphill side of the nozzle (at 0 degrees), Figure 10 indicates that the residual stresses would become compressive once this crack reaches a crack length of 260 degrees (since through-wall cracks grow at two ends, this is indicated on Figure 10 as a half crack length of 130 degrees).

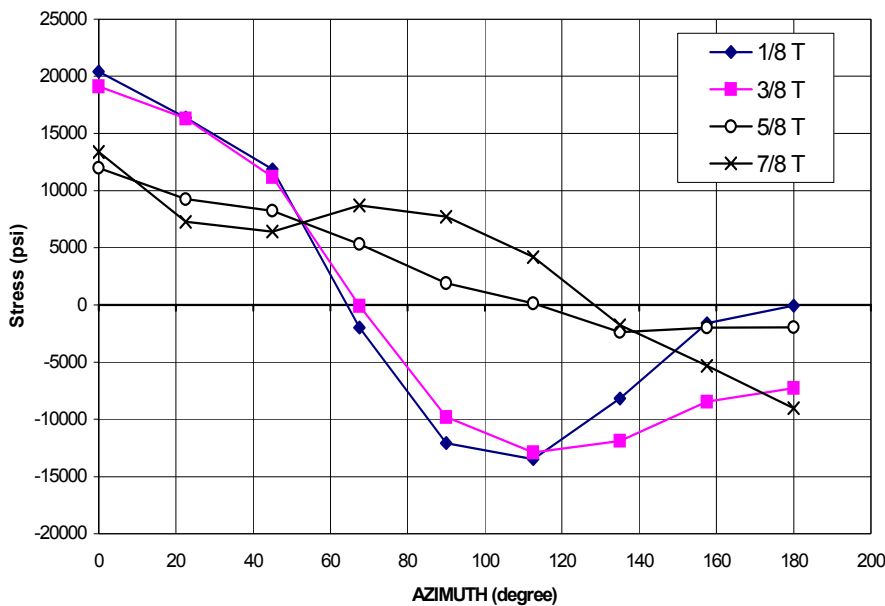


Figure 10 Axial through-thickness residual stress profile for CRDM nozzles.

There are potential issues with the weld residual stress analysis that could have an effect on the resultant residual stresses. These include the precise weld simulation procedures (e.g., whether each weld pass was created at the same time in the simulation or as a traveling arc where the material surrounding the weld arc acts as heat sink in front and behind the arc, in addition to normal to the welding direction), the hardening modeling used (e.g., elastic perfectly-plastic stress strain behavior or non-linear strain hardening), the progression used to generate the weld (e.g., ring-like steps or welding from the uphill side to the downhill side in two separate

operations for each half circumference), and the fill order (e.g., starting from the RPV head and working to the tube or from the tube and working out).

4.2.1.3 Thermal Expansion Differences

After the head has been fabricated and put into service, the operating conditions of temperature and pressure will affect the interfacial relationship of the nozzle and the RPV head, and should be considered in RPV head analyses. The pressure stresses on the head will cause the holes in the head to expand, and multiple holes will make that expansion greater than if a single hole is considered in the analysis. The difference in the thermal expansion of the low alloy head material and the Alloy 600 tubing will also cause the hole to expand relative to the tube. This relative expansion behavior is a positive aspect in that it will promote coolant leakage through the annular “interference fit” area of the nozzle. However, this relative expansion will also cause a stress concentration at the root of the weld that will contribute to the crack-driving force at that geometric discontinuity. These stress components are thermal expansion and pressure driven; hence, they might be relatively uniform around the circumference of the tube. If great enough, they may contribute to multiple crack initiation sites. Although the mode I crack-driving force for this case would cause the crack to grow along the nozzle/weld interface, those stresses in combination with the weld residual stresses may cause a crack-driving-force contribution that might be greater than using just the stresses in the longitudinal direction of the tube. The principal stresses in the axial plane of the tube and through the weld would have to be examined to understand this better. It is not known how this consideration has been included in the industry weld residual stress analyses and whether this has been included in the fracture model.

4.2.1.4 Cyclic Thermal Stresses

Thermal-hydraulic analyses for the Ringhals plant indicate that there is a thermal transient in the nozzle around the weld area (Ref. 29). This thermal transient comes from the mixing of hot and cooler water in the nozzle from below and above the weld. These thermal loads were not thought to be large enough to cause cracking by themselves, but may add a cyclic component to the stresses currently considered in the analyses. It was noted that, “This could be one of the probable explanations why the cold-dome is affected by PWSCC earlier than expected.” Results in other industries have shown that SCC can be accelerated with small cyclic loading having R-ratios (minimum/maximum stress ratios) of 0.95. This aspect may be more important to internal axial cracking than the external axial cracking that occurred at Oconee.

At this time there is insufficient analysis of this phenomenon to include it in the assessment of VHP nozzle cracking. As the analyses for VHP nozzle cracking become more detailed and additional information becomes available, inclusion of these stresses should be considered.

4.2.2 Crack-Driving Force Analyses

The crack-driving force for PWSCC comes from the stresses that were discussed previously. In this evaluation, the crack-driving force is characterized by the stress-intensity factor K , which is related to the stress field around the crack tip. For a circumferential crack in a CRDM nozzle, these have not been examined before. As indicated in Figure 11 (Ref. 28), the crack-driving force on the uphill side of the nozzle exceeds that at the downhill side for all crack angles. For the uphill side, the crack-driving force reaches a minimum at about 260 degrees, and then

increases as the crack size increases. Note that these preliminary results did not include pressure on the crack faces.

4.3 On-Going NRC-Funded Efforts

As part of a review by an independent group of experts convened by the NRC Office of Nuclear Regulatory Research (RES) summarized in Ref. 30, initial calculations to determine the magnitude of the crack-driving force, crack-opening displacements, leak rates, and critical flaw sizes were made both at Engineering Mechanics Corporation of Columbus (Emc²) and Oak Ridge National Laboratory (ORNL), as summarized in Refs. 31 and 32, respectively.

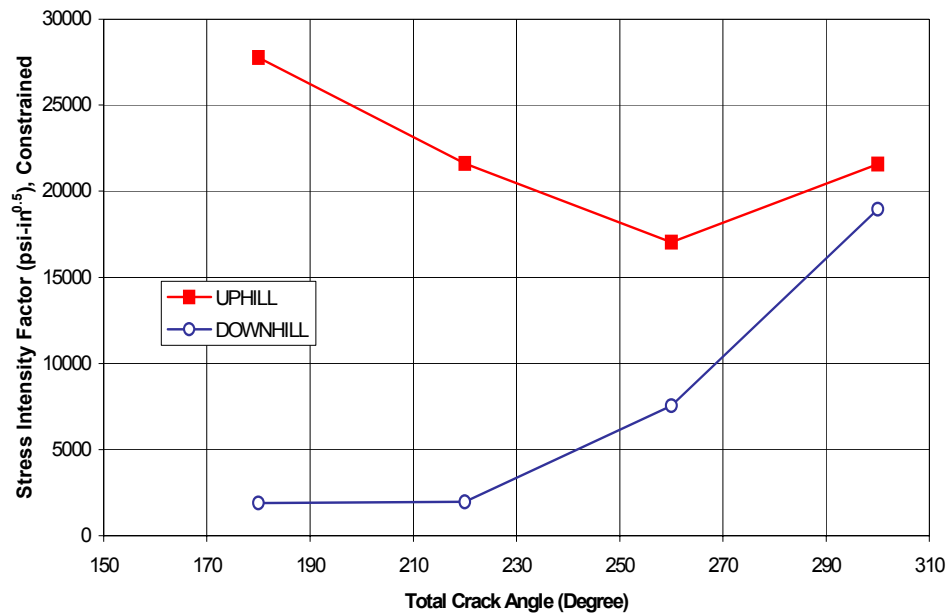


Figure 11 Illustration of crack-driving forces for circumferential cracks in CRDM nozzles

Although weld residual stress analyses results are not available yet, there are plans to assess the effects of weld sequencing on the variability of the residual stresses. Since the whole stress and strain fields will be mapped onto a model containing a crack, the effects of redistribution of the residual stresses can be more accurately determined than in the industry efforts described previously.

Of the initial short-term efforts conducted to date, the effect of pressure loading alone on the crack-opening displacement and crack-driving force were conducted with the boundary conditions appropriate for a CRDM nozzle. In the CRDM nozzle, the pressure loads can cause an axial load, termed the end-capped loads, as well as pressure on the crack faces. ORNL conducted 3D elastic-plastic analyses of a CRDM nozzle with gap elements that simulated the rotational restraint from the “interference-fit” region assuming a gap of 0.03 to 0.05 mm (0.001 to 0.002 inch) at the operating temperature conditions in the “interference-fit” region, and included the end-capped load as well as pressure on the crack faces. The ORNL results showed sufficiently low K values that they were considered representative of elastic behavior for

the crack sizes examined. Emc² conducted elastic analysis that used boundary conditions to restrain the pipe rotation, which should effectively behave the same as using the gap elements that ORNL used. The Emc² results included the end-capped loads, but no pressure on the crack faces. Emc² also examined unrestrained conditions for various crack lengths. Figure 12 shows the stress-intensity factor (K) versus total circumferential crack angle from the ORNL and Emc² results. Note the higher K values for the unrestrained conditions, especially for longer crack lengths.

By subtracting the Emc² K values from the ORNL K values for the restrained cases, the K values from only the crack-face pressure (with the full pressure of 15.3 MPa (2,220 psig) across the whole crack face) could be determined. Several possible pressure conditions could exist in the crack face area:

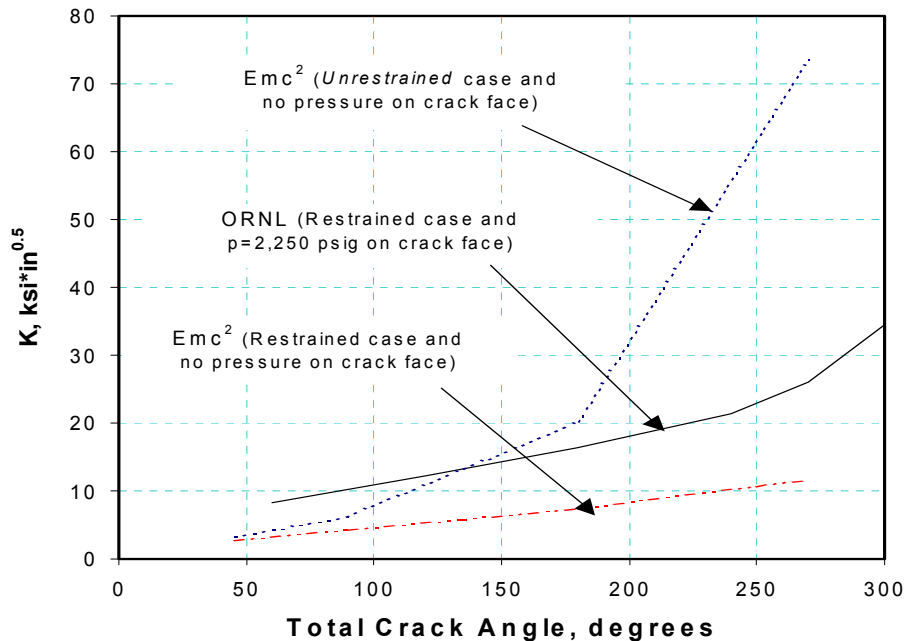


Figure 12 Crack-driving force (K) versus total crack angle from 15.3 MPa (2,220 psig) pressure in typical CRDM. (The restrained condition is representative of CRDM with interference fit. The unrestrained condition is the typical boundary condition for solutions that are also in the literature for a pipe with endcap loading.)

- (1) If the water flow through the crack and annular interference fit region was not blocked, then the pressure at the exit plane (OD of the tube) of the CRDM crack would be less than the vessel internal pressure.
- (2) If there is flow blockage in the annular space in the “interference-fit” region, then the pressure could have the vessel internal pressure across the entire crack face.

- (3) If the flow blockage is in the crack plane, then the crack-face pressures could be lower than the vessel internal pressure.

The most conservative assumption for the crack growth calculations is to assume the crack-face pressure is constant at the vessel internal pressure.

In Ref. 7, the relative effects of weld residual stresses and pressure-induced stresses on crack-driving forces were evaluated for a range of circumferential through-wall crack lengths in a CRDM nozzle penetration. In Step 1 of that analysis, the 3-D finite-element model of the circumferential through-wall flaw is closed (i.e., no flaw) and a fixed displacement is applied to the far end of the CRDM nozzle. The magnitude of the displacement induces a uniform axial elastic tensile strain that corresponds to an estimate of the average axial residual stress of 13.8 MPa (20 ksi) discussed in Section 4.1. In Step 2, the flaw is released while the axial displacement is maintained. In Step 3, the internal pressure is applied to the inside walls of the nozzle and across the open crack face. Figure 13 presents a comparison of crack-driving force versus internal pressure loading for a range of flaw angles with and without simulated residual stresses included in the loading state. In Figure 14, the computed crack-driving force versus angle subtended by the circumferential crack is plotted with and without residual stresses for an internal pressure of 15.3 MPa (2220 psi). Since the estimated residual stresses are in the elastic region, all of the elastic strain energy imparted into the full length of the nozzle during Step 1 is available to open the flaw in Step 2. Thus, the analysis over-estimates the total magnitude of elastic strain energy in the nozzle, since it is expected that the residual stresses will be heavily localized in the region of the J-groove weld and not distributed across the full length of the nozzle. Analysis results described in Ref. 7 indicate a relaxation of the dominant residual stresses with increasing crack length, a trend that is expected to be more pronounced in a more realistic model of the process.

Although weld residual stress analysis results from NRC-sponsored studies are not available yet, there are plans to assess the effects of weld sequencing on the variability of the residual stresses. Since the whole stress and strain fields will be mapped on to a model containing a crack, the effects of redistribution of the residual stresses can be more accurately determined than in the industry efforts described previously.

4.4 Staff Conclusions

The preliminary results from SIA given in Section 4.2 are available only for angles from 175° to 300°. This solution was extended to a wider range of crack angles by matching the ORNL solution for the K due to internal pressure discussed in Section 4.3 at large crack angles where it can be assumed that the pressure loading dominates K. At small angles, extrapolation of the SIA results was fairly consistent with estimates by ORNL of a K of about 66 MPa√m (60 ksi√in.) due to residual stresses for a crack angle of 90°. The stress intensity decreases to zero as the crack angle decreases to zero. The resulting estimate of K is slightly more conservative than the SIA results for the range over which finite element method (FEM) results are available as shown in Figure 15. These results will vary from nozzle to nozzle, but until more results are available, it is assumed that Figure 15 gives a reasonable, conservative representation of K.

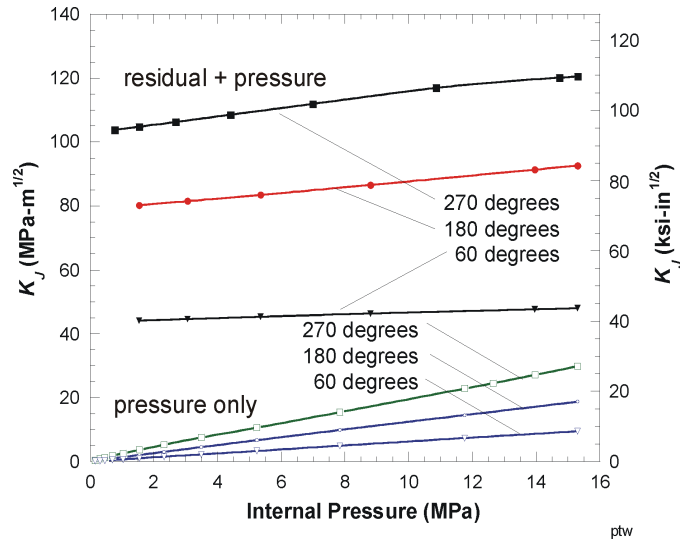


Figure 13 Comparison of K_J values calculated with and without simulated residual stress load. K_J values for total flaw lengths of 60°, 180°, and 270°.

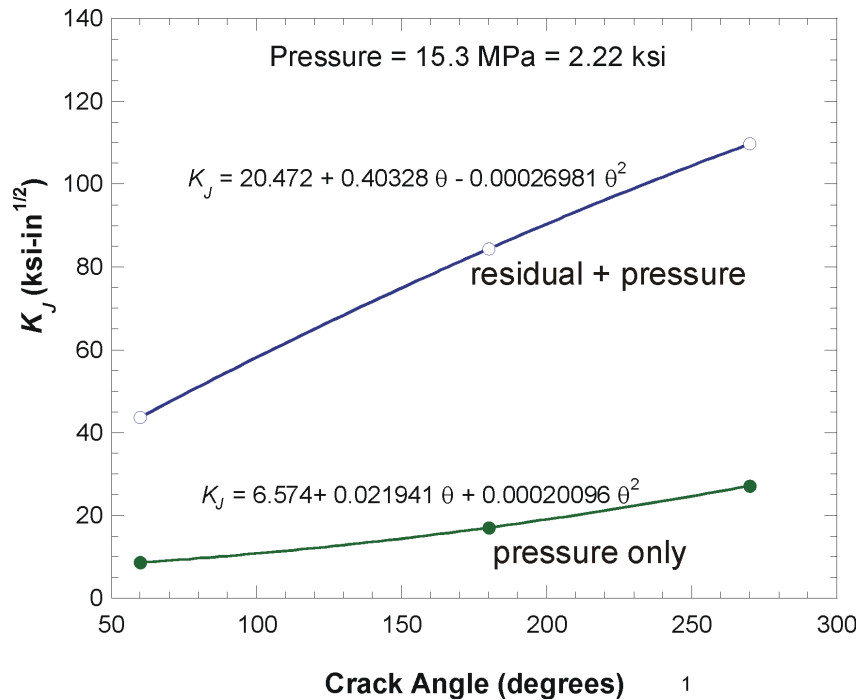


Figure 14 Crack-driving forces versus crack angle resulting from combined residual and pressure-induced stresses and from pressure-induced stresses only. The internal pressure is 15.3 MPa (2,220 psi).

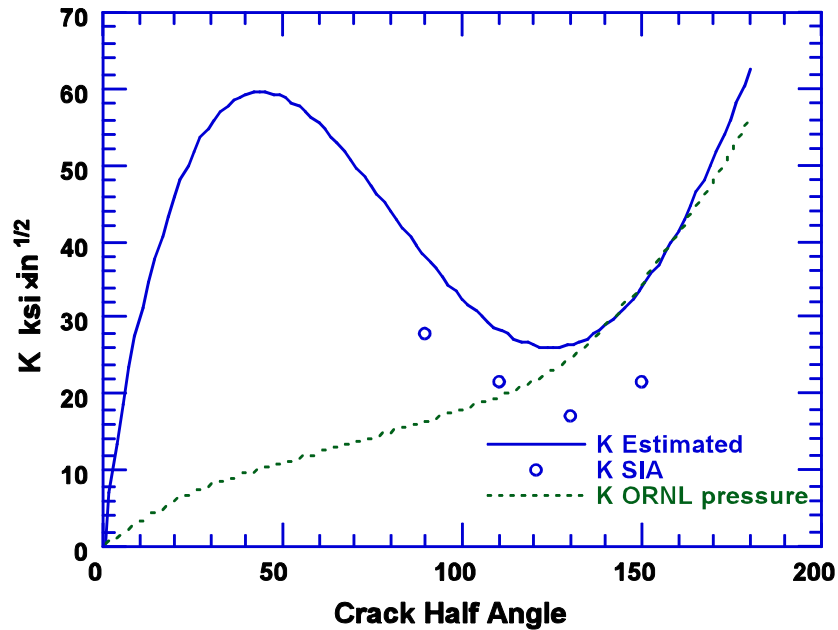


Figure 15 Estimated stress intensity factor K for a CRDM nozzle based on SIA and ORNL results.

5.0 CRITICAL CRACK SIZE

The MRP documented its interim safety assessment in the MRP-44 Part 2 report (Ref. 8). This report includes an analysis of through-wall circumferential cracks above the J-groove weld to determine the margin that existed in the ONS-3 CRDM nozzles at the time that the cracks were detected. The MRP employed a limit-load analysis to determine the maximum permissible crack size at three times the design pressure of 17.2 MPa (2500 psi), consistent with ASME Code margins, for the limiting incore instrument (ICI), control element drive mechanism (CEDM) and control rod drive mechanism (CRDM) nozzles throughout the PWR industry. The maximum permissible crack size for limit-load at three times the design pressure was 179° for the ICI nozzles, 244° for the CEDM nozzles, and 273° for the CRDM nozzles.

Emc² performed a review of the critical circumferential crack length for CRDM nozzles including the appropriateness of the limit-load equation that was used in MRP-44, Part 2 (Ref. 8). This analysis used both the ASME Code strength values for Alloy 600 at 315°C (600°F) and available data for an Alloy 600 tube tested at 288°C (550°F). The review concluded that the limit-load analysis is a valid approach for determining the critical circumferential crack length in the CRDM nozzle geometry using Alloy 600 material. The calculation with full internal pressure on the crack face and the safety margin of three applied to primary loads results in critical crack lengths between 262° and 269°, depending on the strength properties used. These values are slightly less than the value determined by the MRP (273°).

The analysis also considered a limit-load calculation to illustrate the effect of a complex crack geometry (e.g., a certain length through-wall crack superimposed on a 360° circumferential

surface crack) on the critical through-wall crack size. For example, a 360° surface crack that is 25 percent or 50 percent of the wall thickness reduces the allowable through-wall crack length to 230° and 165°, respectively.

The allowable pressures for a variety of crack geometries (including a through wall crack and several complex crack geometries) as a function of the through-wall crack length is provided in Figure 16. For the case of the surface crack length being zero (e.g., a through-wall crack only)

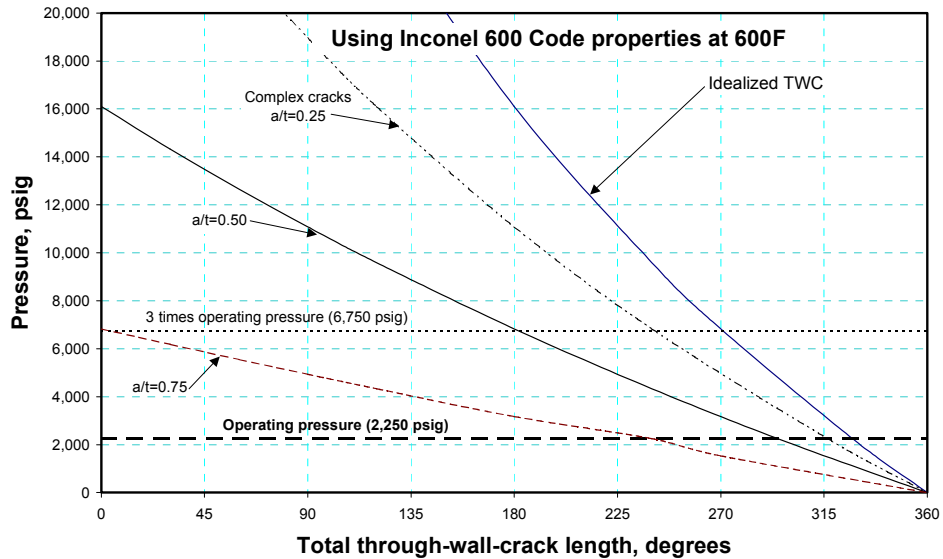


Figure 16 Calculated failure pressures as a function of through-wall crack length for a variety of crack configurations. For a through-wall crack only, the critical crack length for nozzle failure is 324°.

and a factor of one applied to primary loads (e.g., no safety margin on applied load), the critical crack length for failure of a CRDM nozzle is 324°. This critical crack length does not consider uncertainties in crack size, material properties (e.g., the strength of the nozzle material), or any other part of the analysis.

Figure 17 shows how the critical flaw dimensions change from an idealized through-wall flaw to a complex crack to a constant depth surface flaw at 17.2 MPa (2,500 psig). The constant-depth surface flaw would have to be 90 percent of the thickness all around the circumference to be critical at 2,500 psig. It is highly unlikely that a surface flaw could grow that deep and maintain a constant depth without penetrating the thickness.

5.1 Staff Conclusions

From the industry and NRC contractor calculations, the critical crack size for a safety margin of three on pressure is 270°, and for nozzle failure/ejection the critical crack size is 324°.

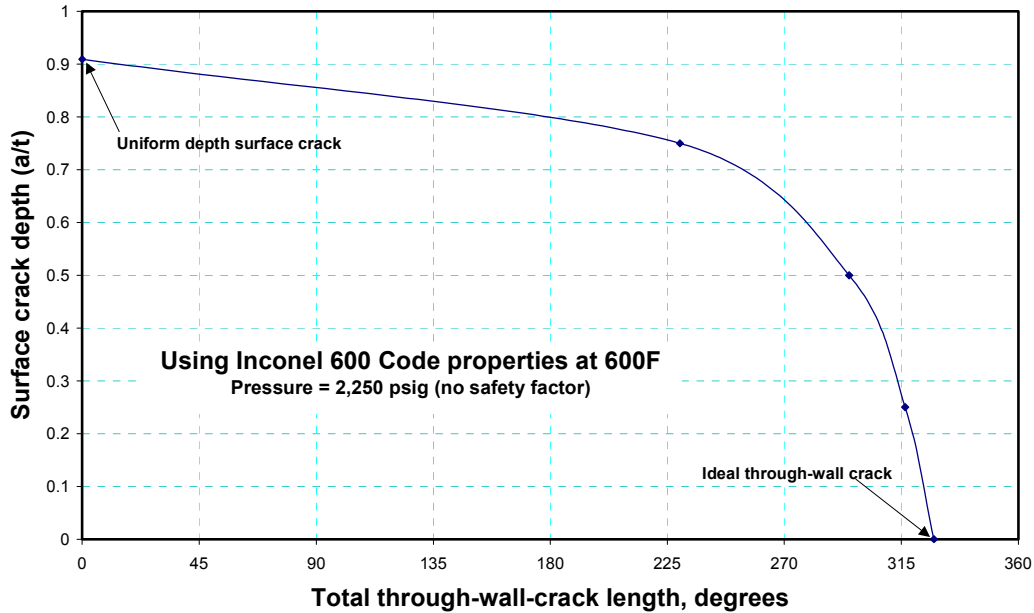


Figure 17 Critical crack sizes in a typical CRDM at 15.5 MPa (2,250 psig).

6.0 DETERMINISTIC ASSESSMENT

6.1 Introduction

Previous sections of this report provided evaluation of available information on crack initiation and crack growth rate data, stress analyses and models applicable to assessing the CRDM cracking phenomena. In this section deterministic analyses of the time to failure for varying initial circumferential crack size along with deterministic sensitivity studies, and evaluation of deterministic margins are provided. Section 8 of this report discusses how this information along with a plant's specific susceptibility to cracking and prior inspection history can be used to inform decisions regarding the appropriate timing of inspections.

6.2 Base Case

The ASME Code, as referenced in Title 10 of the Code of Federal Regulations (10 CFR) Part 50.55a, does not allow through wall leakage. The deepest cracks allowed by the ASME Code would not exceed 75 percent of the wall thickness either for axial or circumferential cracks. Cracks that are evaluated as acceptable must have factors of safety of three against failure under operating conditions. Thus, any leakage which indicates a through-wall flaw would not satisfy the requirements of either 10 CFR 50.55a or the ASME Code, and would violate technical specification requirements that preclude pressure boundary leakage. Although these requirements are intended to preclude through-wall cracking and leakage, the high ductility characteristic of VHP nozzle materials mean that significant margins against failure can still exist even in the case of through-wall circumferential cracks. Thus, the staff has performed an

analysis to understand the deterministic margins associated with the VHP nozzle cracking mechanism.

The parameters associated with these deterministic analysis are the initial crack size, the crack growth rate for circumferential cracks, and the critical crack size. As discussed in Sections 3 and 5, there are sufficient data available to evaluate pertinent crack growth rates and critical crack size. However, the lack of sufficient data from inservice inspections and the large uncertainties associated with crack initiation evaluations lead to a limited ability to provide reliable estimates of initial crack size. Therefore, the approach taken in this section is to define a base case utilizing a specified crack growth rate to calculate the operating time prior to reaching the critical crack size corresponding to a factor of safety of three against failure, consistent with the intent of the ASME Code, and also the time to reach a critical crack size that result in nozzle failure and probable ejection. These evaluations are made with a variety of circumferential crack sizes. Sensitivity studies on assumed crack growth rate and a discussions of uncertainties in the deterministic assessment are also presented.

It is expected that these analyses will be refined and expanded in the future as additional relevant data become available.

6.2.1 Assumed Critical Flaw Size

As described in Section 5, the critical flaw size can be determined in two ways, as either that flaw size which satisfies a margin of three on design pressure (consistent with the requirements of Section XI of the ASME Code), or the flaw size at which structural failure of the VHP nozzle would occur under normal operating conditions, possibly leading to ejection of the nozzle. As described in Section 5, estimates of the critical flaw size with a safety margin of three on the design pressure range from 262° to 269° from calculations by NRC contractors to 273° from industry calculations, and the critical flaw size for nozzle failure/ejection is 324° from calculations by NRC contractors and 330° from industry calculations. Note that these calculations assume there is not a surface flaw in the same plane as the through-wall flaw. As described in Section 5, a surface flaw in the crack plane would reduce the critical through-wall crack length, and if the surface flaw has a constant depth of 90-percent of the thickness, it would be critical with no through-wall crack. The growth of a surface flaw to such a large depth and having a critical depth without a through-wall component of the flaw is unlikely, so that there should be some through-wall leakage prior to failure.

The flaw size determined using the margin of three on design pressure is used in the base case deterministic analysis. Traditionally, a safety margin is intended, in part, to compensate for uncertainties, such as material properties, unanticipated loadings, etc. This use comes with the additional knowledge that the actual failure of the VHP nozzle would be expected to occur at some time period after reaching that flaw size. The effectiveness of a factor of safety of three in accounting for the variability in parameters such as crack growth rate is discussed as part of the sensitivity studies.

For the base case deterministic evaluation, the staff has used a failure/ejection circumferential crack length of 324°, and a crack length of 270° for a margin of three on the design pressure.

6.2.2 Assumed Crack Growth Rate

As described in Section 3, there are no crack growth data for conditions, e.g., material and test conditions (environment and temperature), directly relevant to VHP nozzle cracking, partly owing to the fact that the environmental conditions in the annulus between the nozzle and the RPV head have not been verified through field experience. In Section 3, it is concluded that the observed crack growth rates in primary coolant water should be representative of the expected crack growth rates, and an analysis of the available data for these conditions is described in Section 3.

For the deterministic calculations, the crack growth rate was evaluated through simplified K-dependent calculations. The deterministic calculations use the Scott model. With the high degree of variability evident in the crack growth rate data, the deterministic evaluation used the crack growth rate parameter A based on a 95/50 statistical evaluation of the data. From Table 3 at an operating temperature of 325°C (617°F), the 95/50 A is 1.8×10^{-11} . However, A is strongly dependent on the operating temperature, and can be adjusted to different temperatures based on the Arrhenius relationship. From a review of the reported RPV head operating temperatures, the staff has used a temperature of 318°C (605°F) for the base case deterministic evaluation. At this temperature, the 95/50 A is determined to be 1.303×10^{-11} . Using the stress intensity results illustrated in Figure 15, the crack growth rate at 318°C (605°F) as a function of circumferential crack size is illustrated in Figure 18. From this figure, the crack growth rates range from 12.7 to almost 51 mm/yr (0.5 to 2 in./yr).

The base case deterministic evaluation determined the crack growth rate for an increment of growth as the average value of the crack growth rate for that increment of growth, e.g., the growth rate from 20° to 30° was determined by averaging the crack growth rate at 20° and 30°. The time for this increment of growth was then determined by dividing the increment of growth by this average crack growth rate for the increment.

Consideration of the crack growth rate at other conditions, including varying the operating temperature and using different statistical bounds to the data, is described in Section 6.3.

6.2.3 Assumed Initial Flaw Size

Definition of the initial flaw size is the single most difficult task of the deterministic analysis. The use of qualified visual examinations to monitor for leakage deposits is at best an indirect indication of the presence of cracking, and may provide no direct tie to the crack length in any degraded nozzle. In addition, follow-up examinations with volumetric examination methods to characterize only those nozzles with detectable leakage deposits, and perhaps a small additional sample of nozzles, do not provide complete data on the population of flaws in nozzles, in that determination of the flaw population for nozzles without detectable leakage are generally not performed.

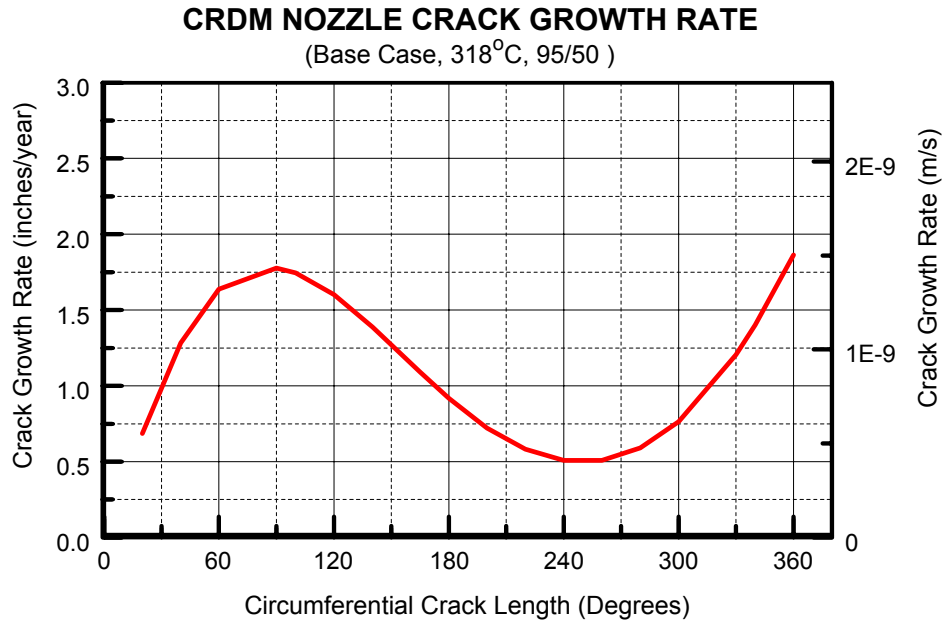


Figure 18 Variation of crack growth rate with circumferential crack length for the base case of 318°C (605°F) 95/50 curve.

That notwithstanding, the available data for OD circumferential flaws from examinations in the Spring and Fall 2001 outages are summarized in Table 4, based on the destructively measured crack lengths for two of the flaws and the ultrasonic (UT) measurements of the other three flaws. From these results there are a variety of sizes for the flaws that have been identified in CRDM nozzles. Based on these results it is possible to say that the largest flaw identified thus far is 165°. However, it should be noted that the only circumferential flaws for which the circumferential lengths has been verified destructively are the pair of 165° cracks at ONS-3, and one of these two flaws was significantly undersized by the UT measurements as 59°, an error by a factor of 2.8 or 106°. The flaw sizes for Crystal River Unit 3, the shorter of the flaws at ONS-3 and the single circumferential crack in ONS-2 are based only on UT measurements. It should be noted that the shorter flaw at ONS-3 was not identified by the UT examination until a third-party review of the data, and hence it was not identified prior to the completion of repairs of the affected nozzle. In the other two cases, the cracks were removed by machining without any additional efforts to determine the actual extent of the cracking in the affected nozzles. Given prior experience with UT examination and the current state of qualification of UT inspections for these components, the actual sizes of these cracks is uncertain.

Table 4 Summary of OD Circumferential Flaws Identified in Spring and Fall 2001 Outages

| Plant | Nozzle ID | Circumferential Crack Length | Through-Wall Extent |
|----------------------|-----------|------------------------------|---------------------|
| Oconee Unit 3 | 50 | 165° | 100% |
| Oconee Unit 3 | 56 | 165° | 100% |
| Oconee Unit3 | 23 | 66° * | 35% * |
| Oconee Unit 2 | 18 | 45° * | 10% * |
| Crystal River Unit 3 | 32 | 90° * | 50% * |

* Crack dimensions estimated from UT data.

It should be noted that the purpose of NRC Bulletin 2001-01, "Circumferential Cracking of Reactor Pressure Vessel Head Penetration Nozzles," was to provide information regarding the extent and severity of cracking occurring in VHP nozzles. The assumption regarding the crack size remaining after a qualified visual examination represents the additional uncertainty that one has in the population of undetected flaws in the VHP nozzles, since the detection of no leakage deposits is not a direct indication of the absence of cracking in the VHP nozzles but only an indication that any cracking that is occurring has not resulted in a detectable leakage deposit on the RPV head.

Conversely, performance of surface or volumetric examinations of 100 percent of the VHP nozzles does provide an opportunity to directly sample the population of flaws that may be occurring in the VHP nozzles, within the detectability and reliability performance characteristics of the examination method. In such cases, the assumption of a smaller initial crack size remaining after examination can be more easily defined and defended based on the performance characteristics of the examination method.

Due to the lack of sufficient inspection data from plants and large uncertainties associated with time to crack initiation, the existing flaw sizes that could exist in plants is unknown. Therefore, the base case deterministic calculations focus on a determination of the operating times necessary to reach the 270° critical flaw size (at three times the design pressure) and the 324° critical flaw size (at nozzle failure/ejection). These operating times are determined as a function of the initial flaw size.

6.2.4 Base Case Results

The results of the analyses performed using the base case assumptions are provided in Figure 19. As illustrated in this figure, nozzle failure/ejection is predicted to occur about 12 months after the various sizes of flaws have reached the critical length at three times the design pressure. As an example, a 180° flaw would reach 270° in about 26 months and the 324° nozzle failure/ejection size in about 38 months.

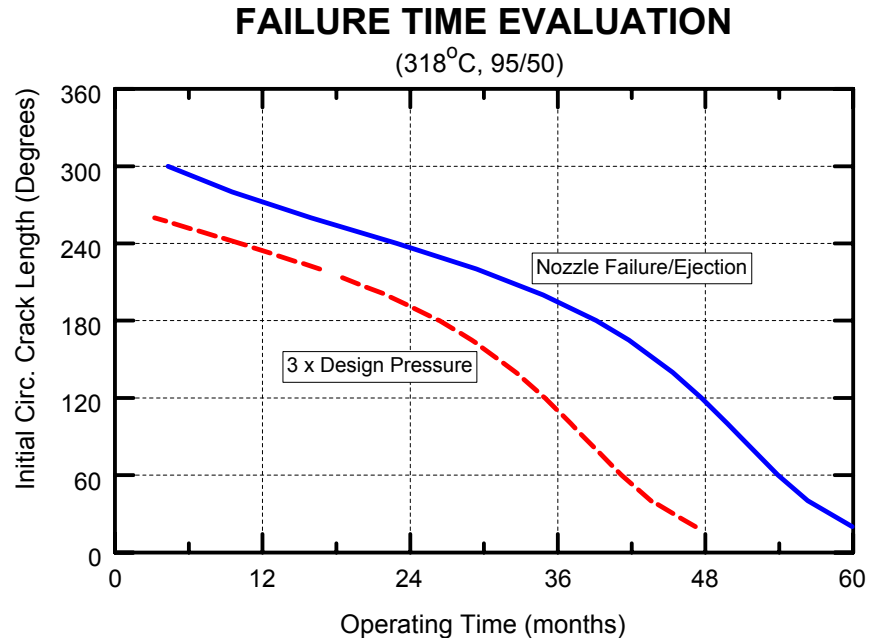


Figure 19 Variation of time to failure as a function of initial crack length, for the base case of 318°C (605°F), 95/50, crack growth rate.

Figure 20 presents the time to failure for a specific initial flaw size of 165°. This case would resemble the Oconee Unit 3 conditions when the two 165° circumferential flaws were identified in Spring 2001. For this base case, the 165° flaw would grow to 270° in approximately 29 months, and to 324° in about 42 months. Note the non-linearity of the crack length curve as a function of operating time, reflective of the variations in crack growth size as a function of the crack size dependent applied stress intensity (K) level.

The evaluation presented in Figure 20 demonstrates the type of deterministic analysis that is normally performed with reliable information regarding the initial flaw size, and also supports the sensitivity studies discussed in the next section.

6.3 Uncertainties and Sensitivity Studies

In the absence of definitive data, the use of parametric values of crack growth rate can provide an understanding of the impact of various assumptions on the evaluation within the context of relevant values of the parameters. For the case of CRDM nozzle cracking, the effect of initial flaw size on the operating time to achieve the critical flaw sizes has been considered in Figure 19. Besides the initial crack size, another key parameter with a high level uncertainty is the crack growth rate.

At least three issues affect the selection of the crack growth rate: the environmental conditions, the operating temperature and the statistical basis for the selected crack growth rate. For OD circumferential cracking in CRDM nozzles, Section 2.1 concluded that PWSCC conditions are a reasonable approximation to the conditions thought to exist in the annulus between the nozzle and the RPV head, and as such crack growth data for PWSCC conditions are used in this

CRACK GROWTH EVALUATION

(Base Case, 318°C, 95/50)

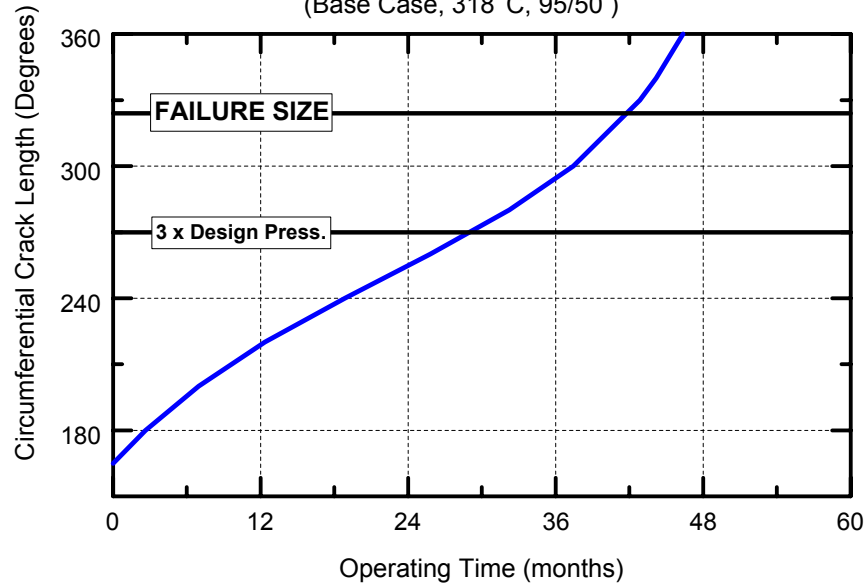


Figure 20 Evaluation of operating time to reach critical flaw sizes at three times design pressure and at nozzle failure/ejection after development of a 165° long circumferential through-wall flaw.

analysis. [As noted in Section 6.2.1, field confirmation of the annulus conditions should be pursued by the industry to eliminate any uncertainty regarding the annulus conditions.]

As described in Section 6.3, the effect of operating temperature on the crack growth rate can be assessed using an Arrhenius relation. For the case of CRDM nozzle conditions, MRP-48 (Ref. 33) indicates that RPV heads are operating in the temperature range from 286°C to 318°C (547°F to 605°F). The base case described in Section 6.2.2 used 318°C (605°F). In addition, the benchmark evaluations of the available crack growth data (see Section 3) have used 325°C (617°F). To illustrate the effects of operating temperature on the crack growth rate, the Arrhenius relation has been used to define the ratio of the A parameter from the Scott model at operating temperature with that at 325°C (617°F), as provided in Figure 21. Referencing from the base case of 318°C (605°F), reducing the operating temperature by 3°C (6°F), to 315°C (599°F), results in a reduction in the crack growth rate of 13 percent. Reducing the operating temperature to 286°C (547°F), the lowest CRDM nozzle operating temperature according to MRP-48 (Ref. 33), the crack growth rate reduces by 80 percent from the rate at 318°C (605°F).

In addition to the temperature at which the crack growth rate is evaluated, the statistical bound used to define the A parameter in the Scott model can also have an effect on the results. As indicated in Section 6.2.2, the base case used a 95/50 statistical evaluation of the data at 318°C (605°F). From Section 6.3, comparison of the 50/50 curve with the field measurements by EDF indicates that the 50/50 curve is less than the mean of the field measurements. One

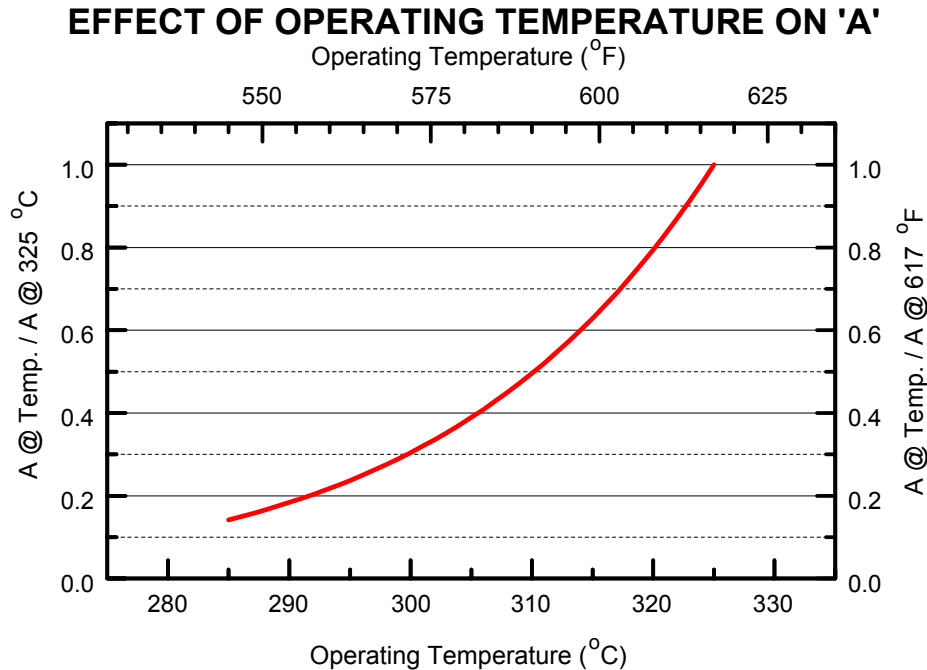


Figure 21 Lower operating temperature results in lower crack growth rates for VHP nozzle materials, within the operating temperature range of the nozzles.

hypothesis to explain this observation is that the heats exhibiting cracking in the field may be relatively higher in susceptibility to PWSCC than the overall population of heats that have been examined in the laboratory, such that the more susceptible materials would tend to crack earlier and more frequently than less susceptible heats, and would thus be disproportionately represented in the population of field data. With Figure 9 as a basis, an approximate mean to data for these "higher susceptibility heats" (that may result in cracking in the field) has been determined as the square root of the products of the 95/50 and 50/50 values for A from Table 3. This value of the "mean" A at 325°C (617°F), 7.47×10^{-12} , can then be adjusted for operating temperature conditions using the Arrhenius relation. The sensitivity to the statistical nature of the crack growth rate curve was evaluated using the 95/50 values, termed in the following figures as "B" for bounding, and these root product mean values, termed "M" in the following figures. The simultaneous effects of operating temperature and statistical nature of the curves are illustrated using 95/50 curves at 325°C (617°F), 318°C (605°F), and 315°C (599°F), along with mean values at 318°C (605°F) and 315°C (599°F).

Figure 22 illustrates the crack growth rates as a function of circumferential crack length for the five cases described above. Although there are reductions in crack growth rate related to decreases in operating temperature, there is a more significant decrease in rate in going from the 95/50 curves ('B' on the figure) to the mean curves ('M' on the figure). A comparison of these results with the crack growth rate used in a Framatome analysis (Ref. 34), a linearized rate of 10 mm/year (0.39 in./year), indicates that the Framatome rate is similar to the mean approximation to the crack growth rates for the higher susceptibility heats.

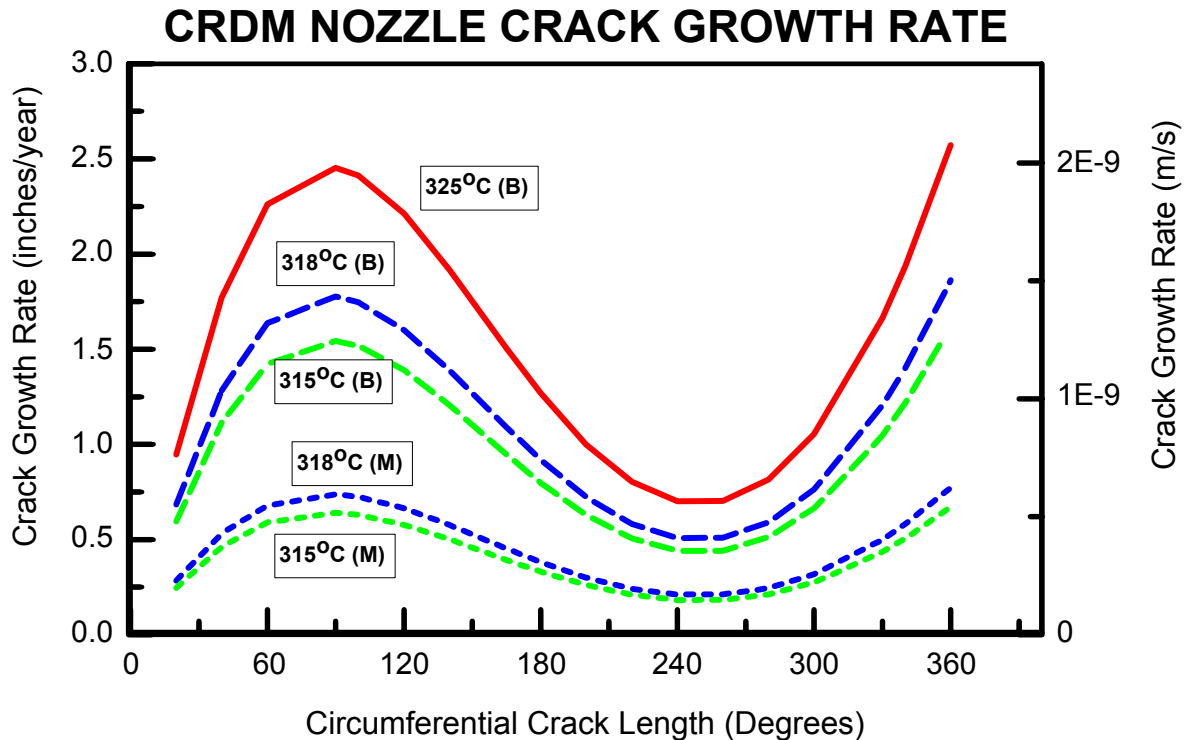


Figure 22 Variation of crack growth rates at several pertinent temperatures and using 95/50 ('B' on the curves) and mean values ('M' on the curves).

Translating these crack growth rates into an evaluation of the time to reach the critical flaw sizes from a 165° initial flaw, Figure 23 illustrates that reducing the temperature and using the 95/50 curves increases the time to reach the three times design pressure curve by up to 12 months and the time to reach the nozzle failure/ejection curve by up to 18 months. However, the most dramatic increase in time is for the mean curve evaluations, where the times to reach the critical flaw sizes increases by 3 to 4 years for the three times design pressure curve and more than 5 years for the nozzle failure/ejection curve.

Applying these crack growth rate curves to determining the time to reach the three times design pressure and the nozzle failure/ejection flaw sizes, the effects of using mean curves instead of the 95/50 curves are very large (Figs. 24 and 25, respectively). At all three temperatures, the 95/50 curves would project that a 60° initial flaw would reach 270° in 3 to 4 years. In contrast, the mean curves do not project reaching this flaw size until more than 8 years of operating time.

Added to these figures are curves for 318°C (605°F) using a 95/95 statistical bound. This curve does not have a high probability, but it does have a possibility of occurring for the VHP nozzles. In this case, the 95/95 curve projects growth of a very small starting flaw to a size that would result in nozzle failure/ejection within 24 months of initiation of the flaw.

CRACK GROWTH EVALUATION

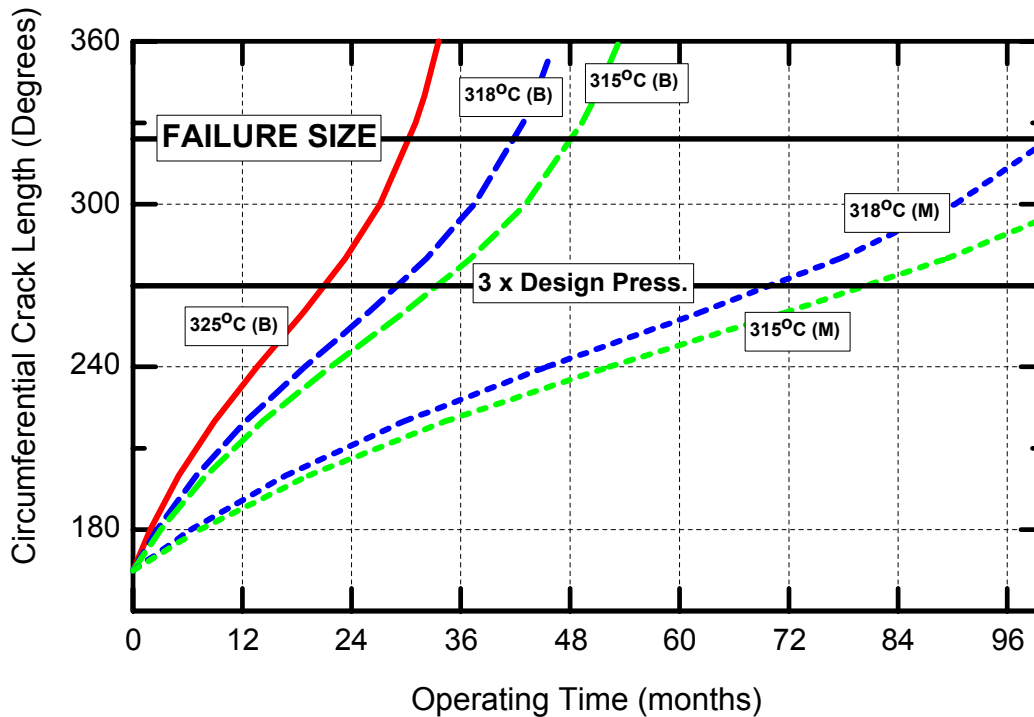


Figure 23 Crack growth analysis using various crack growth rate assumptions, from an initial flaw size of 165°. Although decreasing the temperature has some effect, the most dramatic increases in failure times occur with the mean crack growth curve instead of the 95/50 curve.

In some engineering analyses the approach is to use mean values of variables such as crack growth rate and then apply factors of safety, e.g., three on pressure stresses, to account for uncertainties and variability in material properties. Figure 23 provides some interesting insights regarding the possible use of a mean value for crack growth rate and a factor of safety of three. First, as previously noted, the figure illustrates that the variability in crack growth rate is very large. The difference in predicted times to reach a 270° circumferential crack, corresponding to a factor of safety of three, is approximately 3.5 years. This has important implications regarding the effectiveness of an assumed factor of safety of three. For example, using the mean crack growth rate curve at 318°C with the "3 X Design Press" curve, would result in an acceptable operating time of approximately 6 years. However, if the crack being analyzed grew at the 95/50 growth rate for 318°C, the crack would reach the actual failure size in approximately 4.5 years. Thus, a larger factor of safety than three would need to be applied when utilizing the mean crack growth rates in order to account for the large variability in crack growth rate.

TIME TO 3 X DESIGN PRESSURE

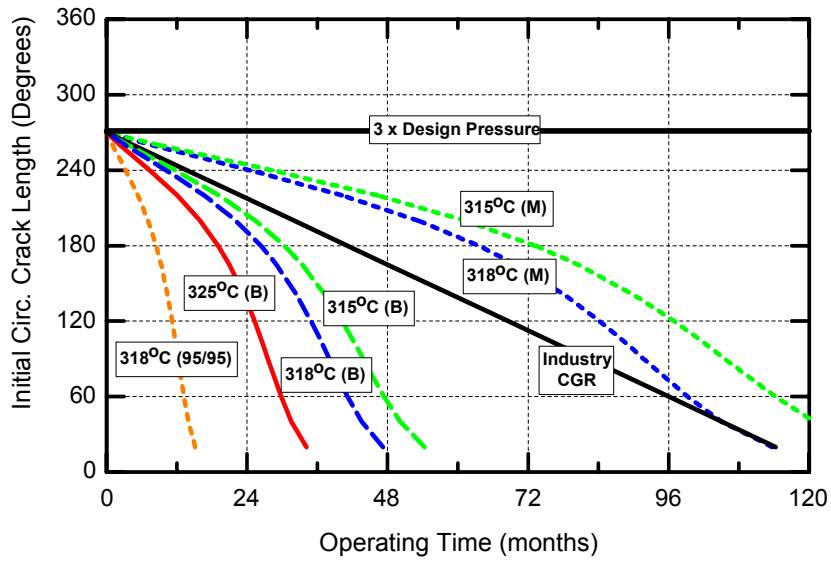


Figure 24 Comparison of time to reach the flaw size representing three times the design pressure, for a variety of crack growth rates and as a function of initial flaw size.

TIME TO NOZZLE FAILURE/EJECTION

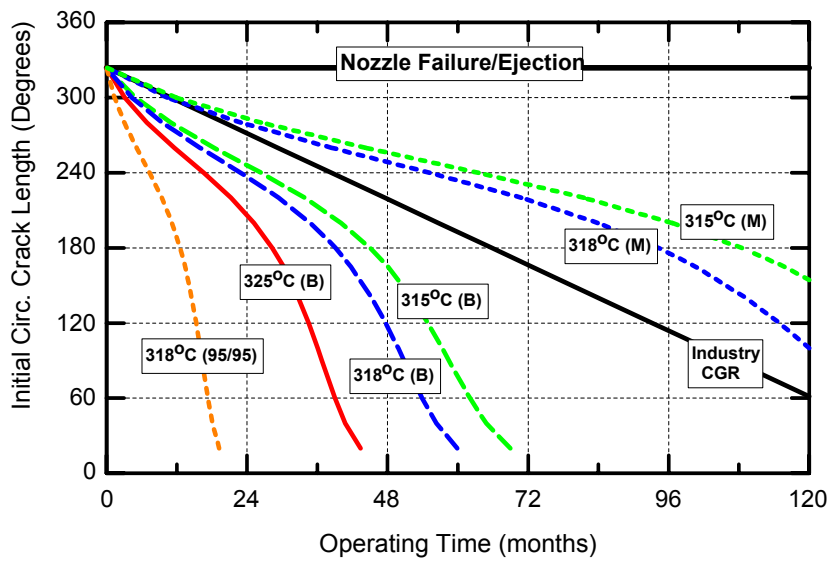


Figure 25 Comparison of time to reach the flaw size representing three times the design pressure, for a variety of crack growth rates and as a function of initial flaw size.

6.4 Conclusions From Deterministic Calculations

From the base case deterministic analysis, nozzles operated at temperatures no higher than 318°C (605°F) could have circumferential flaws grow from a very small size to a size that would not sustain a safety margin of three on the design pressure within about four years from the initiation of the flaw. Continued growth of this flaw for another 12 months would result in the flaw reaching a size that could result in a failure of the nozzle and nozzle ejection. These conclusions are based on a 95/50 crack growth curve. Using a mean curve for the high susceptibility materials would give operating times of 10 years or more from the initiation of cracking, whereas using a 95/95 crack growth rate curve would predict acceptable operating times of two years or less.

As indicated above, the variability in crack growth rates for Alloy 600 in PWSCC conditions is very large and results in significant differences in predicted times to failure based on various assumed statistical growth rate values. A traditional factor of safety of three on design pressure may not be sufficient to account for the large variability in growth rates for PWSCC in CRDM nozzles.

The growth rate of PWSCC cracks in CRDM nozzles is also very sensitive to the operating temperature of the component. As illustrated in Figures 24 and 25, the effect of decreasing the operating temperature by 3°C (5°F) can reduce the projected failure times by six months or more. The sensitivity of the crack growth rate to operating temperature indicates the need to confirm the RPV head operating conditions that are assumed for each plant.

7.0 PROBABILISTIC ASSESSMENT

Application of the results of the deterministic assessments described in Section 6.2 requires making important assumptions such as the sizes of flaws that could exist at various times in the life of a plant and appropriate statistical values to use for crack growth rates. Probabilistic assessments can provide valuable insights that can assist in making these assumptions and for effectively applying the results of the deterministic analyses. Assessments of particular interest include: 1) an assessment of the statistical distributions associated with the number and size of cracks expected at any time in the life of a plant, and 2) an assessment of the probabilities of failure associated with the various failure curves presented in Section 6.2.

One approach to the first assessment would be to model the entire cracking process from initiation of inside surface cracks in the J-groove weld or inside diameter of the VHP nozzle to development and growth of circumferential cracks. However, this approach requires a better understanding than currently exists of the complete cracking process, and additional data to support constructing such a model. An alternative approach is to assess the number and size of cracks based on in-service inspection data. The empirical approach appears more promising at this time than trying to construct a complete phenomenological model; however, it also has limitations, in this case the availability of reliable inspection data. The major challenge with the latter approach is acquiring sufficiently reliable data on the number and size of cracks found in service such that it is possible to determine the appropriate forms and parameters of statistical distributions to use. Acquiring reliable data on the size of cracks is limited because of the current state of qualification of volumetric examination methods with regard to sizing, and the high cost of destructive examinations to determine crack sizes. The staff has initiated work in

this area and will continue to pursue these approaches as the industry and on-going research activities provide more data.

The assessment of the probabilities of failure associated with the various failure curves presented in Section 6.2 is more straight-forward since the only random variable involved is crack growth rate, and sufficient data exist for that variable to perform meaningful statistical analyses. The staff is currently developing an analysis to provide the failure probabilities associated with the failure curves developed in the deterministic analyses. Of course, these probabilities will be conditional on the initial flaw size.

Ultimately, analyses such as those described above need to provide frequencies of failure (rather than probabilities) that can be used with estimates of the conditional core damage probability in a decision-making process similar to that of Regulatory Guide 1.174, "An Approach for Using Probabilistic Risk Assessment in Risk-Informed Decisions on Plant-Specific Changes to the Licensing Basis." It is important to continue to pursue these types of analyses in order to support development of the long term programs for managing VHP nozzle cracking.

8.0 INSPECTION TIMING

The results of the analyses presented in Section 6 are intended to help inform decisions regarding both the initial and subsequent timing of inspections. Several important assumptions are necessary to make such an assessment. This section provides a discussion of some of the key considerations involved in such evaluations.

In order to use the results presented in Section 6, one must first assess whether or not it is reasonable to assume that a circumferential crack exists in a VHP nozzle at a plant. NRC Bulletin 2001-01 assumed that there is a high likelihood that cracking could be occurring in plants exhibiting high susceptibility to PWSCC as evidenced by a susceptibility ranking of less than 5 EFPY from the ONS-3 condition. Results of inspections performed support this assumption. As of November 3, 2001, 8 of 9 high susceptibility plants (including one moderate susceptibility plant) that have performed inspections have detected cracking, and three of these plants had circumferential cracking. Therefore, it is reasonable to assume that some degree of circumferential cracking may exist in high susceptibility plants that have not performed inspections. Results from inspections planned at moderate susceptibility plants will provide data that can be used in the future to assess that category of plants.

High susceptibility plants that have performed effective inspections (e.g., qualified visual, surface or volumetric examinations of 100 percent of the VHP nozzles), and have affected repairs of leaking nozzles, should have a higher level of assurance that the cracking has not progressed to the point of through-wall cracking and development of circumferential cracks in the remaining unrepaired nozzles. However, it should be recognized that new circumferential cracks could develop in the next operating cycle.

Thus for high susceptibility plants that have performed inspections, Figures 23 through 25 can be used to determine the necessary inspection frequency. Of course, it must be decided what level of confidence on the crack growth model is appropriate. For example, utilizing the 95/50 curve for 318°C and assuming that any circumferential crack that may have been returned to service was small or that a circumferential crack just initiated when the plant was returned to

power, Figure 24 would indicate that an inspection frequency of approximately 48 months, while the 95/95 curve would indicate an operating time of between inspection of less than 24 months. These curves can be used to assess what initial flaw size could grow to exceed the size that would meet the factor of safety of three on design pressure or grow to failure during the period of time between the last inspection and the proposed next inspection. It is expected that these types of evaluations, along with additional information regarding the reliability of various types of inspections, will be useful in developing long term inspection strategies.

For high susceptibility plants that have never performed an inspection, it is difficult to apply the results presented in Figures 23 through 25. Without some baseline inspection and absent reliable models to predict the time to crack initiation, there is little basis to assume a circumferential flaw size that could exist at a given point in time.

An important aspect of the evaluations described above is determining what level of confidence should be given to inspections. Expanding on the discussion in Bulletin 2001-01, the use of a qualified visual examination of 100 percent of the VHP nozzles represents the only “above-the-head” examination that is sufficient for detecting the existence of conditions that could lead to circumferential cracking of VHP nozzles. The qualified visual examination includes (1) a plant-specific analysis (using as-built dimensions or appropriate surrogates) which demonstrates that each nozzle has a leakage path that would permit deposits from through-wall nozzle cracking to become available on the RPV head for detection, and (2) implementation of a visual examination that is capable of detecting small boron deposits at the interface between the nozzle and the RPV head. This visual examination, sometimes called a “bare-metal visual examination,” requires access to the bare metal where the nozzle enters the RPV head, and the effectiveness of this visual examination must not be compromised by the presence of insulation, existing deposits on the RPV head, or other factors that could interfere with the detection of deposits indicative of primary coolant leakage from VHP nozzles.

Should the implementation of a qualified visual examination be impossible due to plant-specific considerations such as insulation configuration or pre-existing boric acid deposits that could mask the presence of deposits from VHP nozzle leaks, or an inability to provide the plant-specific analysis that would demonstrate leakage paths for each VHP nozzle, then implementation of “under-the-head” examination methods such as surface examinations (e.g., eddy current) or volumetric examinations (e.g., ultrasonic test) would provide reasonable assurance of the condition of the VHP nozzles for which the qualified visual examination cannot be performed.

The scope of inspections performed is also an important subject. The scope of inspections should include 100 percent of the nozzles and cover the entire surface or metal volume of interest. The surface of interest includes the “wetted surface” that comes into contact with the primary coolant during plant operation, including the nozzle inside diameter, the outside diameter below the J-groove weld, and the surface of the J-groove weld itself. This wetted surface examination is considered acceptable because it adequately addresses the first step of the multiple steps required to produce an OD circumferential crack above the J-groove weld, specifically the presence of leakage into the annulus via a through-wall crack. For a volumetric examination, the principal volume of interest is the OD of the nozzle above the J-groove weld, as a direct demonstration of the absence of such cracking.

For visual examinations completed by licensees prior to issuance of the Bulletin, the reliability of the visual examination as a qualified visual examination (as described above) can occur ex post facto with the successful demonstration of the presence of leakage paths in the nozzles using a plant-specific analysis. An inability to qualify the visual examination would place the plant in the same category as those plants that have not previously performed an examination of their VHP nozzles.

9.0 REFERENCES

1. Presentation by P. Scott at Meeting of MRP Crack Growth Review Team for Alloy 600 and Alloy 182, Arlie, VA, October 2-4, 2001. (Proprietary)
2. P. Berge, D. Noel, J. M. Gras, and B. Prioux, "Chloride Stress Corrosion Cracking of Alloy 600 in Boric Acid Solutions," Proc. Eighth International Symposium on Environmental Degradation of Materials in Nuclear Power systems—Water Reactors, Amelia Island, FL, American Nuclear Society, LaGrange Park, IL (1997).
3. EPRI TR-104811-V1, "PWR Molar Ratio Control Application Guidelines, Volume 1, Summary," Electric Power Research Institute, Palo Alto (1995). (Proprietary)
4. C. A. Campbell and S. Fyfitich, "PWSCC Ranking Model for Alloy 600 Components," Proc. Sixth International Symposium on Environmental Degradation of Materials in Nuclear Power Systems—Water Reactors, San Diego, CA, The Minerals, Metals, and Materials Society, Warrendale, PA (1993).
5. G. V. Rao, "Methodologies to Assess PWSCC Susceptibility of Primary Component Alloy 600 Locations Pressurized Water Reactors," Proc. Sixth International Symposium on Environmental Degradation of Materials in Nuclear Power Systems—Water Reactors, San Diego, CA, The Minerals, Metals, and Materials Society (TMS), Warrendale, PA (1993).
6. P. Scott, "Prediction of Alloy 600 Component Failures in PWR Systems," Research Topical Symposia Part 1 – Life Prediction of Structures subject to Environmental Degradation, National Association of Corrosion Engineers (NACE), Houston, pp 135-160 (1997).
7. Y. S. Garud and R. S. Pathania, "A Simplified Model for SCC Initiation Susceptibility in Alloy 600, with the Influence of Cold Work Layer and Strength Characteristics," Proc. Ninth International Symposium on Environmental Degradation of Materials in Nuclear Power Systems—Water Reactors, The Minerals, Metals, and Materials Society (TMS), Warrendale, PA (1999).
8. "PWR Materials Reliability Program, Interim Alloy 600 Safety Assessments for US PWR Plants (MRP-44): Part 2: Reactor Vessel Top Head Penetrations," EPRI, Palo Alto, CA: 2001. TP-1001491, Part 2.
9. Z. Szklarska-Smilowska and R. B. Rebak, "Stress Corrosion Cracking of Alloy 600 in High Temperature Aqueous Solutions: Influencing Factors, Mechanisms and Models," in Control of Corrosion on the Secondary Side of Steam Generators, Eds. R. W. Staehle, J. A. Gorman, and A. R. McIlree, NACE International, Houston, TX (1996).
10. S. Majumdar, "Assessment of Current Understanding of Mechanism of Initiation, Arrest, and Reinitiation of Stress Corrosion Cracks in PWR Steam Generator Tubing," NUREG/CR-5752 (2000).

11. G. L. Webb, "Environmental Degradation of Alloy 600 and Welded Filler Metal EN82 in an Elevated Temperature Aqueous Environment," Proc. Sixth International Symposium on Environmental Degradation of Materials in Nuclear Power Systems—Water Reactors, San Diego, CA, The Minerals, Metals, and Materials Society (TMS), Warrendale, PA (1993).
12. R. Bandy and D. van Rooyen, "Quantitative Examination of Stress Corrosion Cracking of Alloy 600 In High Temperature Water." Nuclear Engineering and Design, Vol. 86, No. 1 pp. 49-56 (Apr 1983).
13. R. W. Staelhe, J. A. Gorman, and K. D. Stavropoulos, "Statistical Analysis of Steam Generator Tube Degradation," EPRI NP-7493, Licensed Material, Electric Power Research Institute, Palo Alto (1991). (Proprietary)
14. V.N. Shah, D.B. Lowenstein, A.P.L. Turner, S.R. Ward, J.A. Gorman, P.E. McDonald, G.H. Weidenhamer, Nuclear Engineering and Design 134, p. 199 (1992).
15. "Response to NRC Review Comments Relating to PWR Materials Reliability Program, Interim Alloy 600 Safety Assessments for US PWR Plants (MRP-44): Part 2: Reactor Vessel Top Head Penetrations," MRP 2001-050, June 29, 2001. (Proprietary)
16. O. K. Chopra, W. K. Soppet, and W. J. Shack, "Effects of Alloy Chemistry, Cold Work, and Water Chemistry on Corrosion Fatigue and Stress Corrosion Cracking of Nickel Alloys and Welds," NUREG/CR-6721 (2001).
17. P. M. Scott and M. Le Calvar, "Some Possible Mechanisms of Intergranular Stress corrosion Cracking of Alloy 600 in PWR Primary Water," Proc. Sixth International Symposium on Environmental Degradation of Materials in Nuclear Power Systems—Water Reactors, San Diego, CA, The Minerals, Metals, and Materials Society (TMS), Warrendale, PA (1993).
18. J. P. Foster, W. H. Bamford, and Raj S. Pathania, "Effect of Materials on Alloy 600 Crack Growth Rates," Proc. Eighth International Symposium on Environmental Degradation of Materials in Nuclear Power systems—Water Reactors, Amelia Island, FL, American Nuclear Society, LaGrange Park, IL (1997).
19. J. Foster and W. Bamford, "Alloy 600 Penetration Crack Growth Program," EPRI TR-105406, Proceedings: 1994 EPRI Workshop on PWSCC of Alloy 600 in PWRs, Part 2, Licensed Document, Electric Power Research Institute, Palo Alto (1995). (Proprietary)
20. T. Cassagne, D. Caron, J. Daret, and Y. Lefevre, "Stress Corrosion Crack Growth Rate Measurements in Alloys 600 and 182 in Primary Water Loops under Constant Load," Proc. Ninth International Symposium on Environmental Degradation of Materials in Nuclear Power Systems—Water Reactors, The Minerals, Metals, and Materials Society (TMS), Warrendale, PA (1999).
21. C. Amazallag and F. Vaillant, "Stress Corrosion Crack Propagation Rates in Reactor Vessel Head Penetrations in Alloy 600," Proc. Ninth International Symposium on Environmental Degradation of Materials in Nuclear Power Systems—Water Reactors, The Minerals, Metals, and Materials Society (TMS), Warrendale, PA (1999).

22. D. Gómez Briceño and J. Lapeña, "Crack Growth Rates in Vessel Head Penetration Materials," Proceedings: 1994 EPRI Workshop on PWSCC of Alloy 600 in PWRs, Part 2, Licensed Document, Electric Power Research Institute, Palo Alto (1995). (Proprietary)
23. P. Lidar, M. Konig, J. Engstrom, and K. Gott, "Effect of Water Chemistry on Environmentally Assisted Cracking in Alloy 600 in Simulated PWR Environments." Proc. Ninth International Symposium on Environmental Degradation of Materials in Nuclear Power Systems—Water Reactors, The Minerals, Metals, and Materials Society (TMS), Warrendale, PA (1999).
24. "External Circumferential Crack Growth Analysis for B&W Design Reactor Vessel Head Control Rod Drive Mechanism Nozzles," Report BAW-10190P, Addendum 1 (Proprietary), B&W Nuclear Technologies, December 1993.
25. "Safety Evaluation for B&W Design Reactor Vessel Head CRD Mechanism Nozzle Cracking," Report BAW-10190P (Proprietary), BAW-10190 (Non-Proprietary), Ed: C. A. Campbell, B&W Nuclear Technologies, May and June 1993.
26. P. M. Scott, "An Analysis of Primary Water Stress Corrosion Cracking in PWR Steam Generators," Presented at the OECD Meeting, Brussels, Belgium, September 16-20, 1991.
27. I. S. Raju and J. C. Newman, "Stress Intensity Factor for Circumferential Surface Cracks in Pipes and Rods under Tension and Bending Loads," ASTM STP 905, 1986, pp. 789-805.
28. "Probabilistic Fracture Mechanics Analysis of CRDM Nozzles," presented by Dr. Peter C. Riccardella, Structural Integrity Associates, September, 2001. (Proprietary)
29. "Scientific Visit Report," to IAEA, by Young-Wan Park, KINS, October 1995.
30. Memorandum from M. E. Mayfield and J. R. Strosnider to S. J. Collins and A. C. Thadani, "Results of Independent Evaluation of Recent Reactor Vessel Head Penetration Cracking," dated September 7, 2001.
31. B. R. Bass and P. T. Williams, "Assessment of Fracture Mechanics Analyses Applied to Cracking in RPV Control Rod Drive Mechanism Nozzles," ORNL report (un-numbered) transmitted to NRC on July 18, 2001.
32. G. Wilkowski, D. Rudland, Z. Feng and Y.-Y. Wang, "Structural and Leakage Evaluations for CRDM Cracking," by Engineering Mechanics Corporation of Columbus, to USNRC, July 20, 2000.
33. "PWR Materials Reliability Program Response to NRC Bulletin 2001-01 (MRP-48)," 1006284, EPRI, Palo Alto, CA, August 2001. (Proprietary)
34. "RV Head Nozzle and Weld Safety Assessment," FRA-ANP 51-5012567-01, September, 2001. (Proprietary)